Bulletin of Earthquake Engineering
https://doi.org/10.1007/s10518-024-01881-5

ORIGINAL ARTICLE

Bi–axially loaded RC beam–column joints and haunch retrofit

Marchisella Angelo[1] · **Muciaccia Giovanni**[1]

Received: 26 April 2023 / Accepted: 21 February 2024
© The Author(s) 2024

Abstract
In this study, seismic bi–axially loaded RC beam–column joints are investigated. An experimental campaign on shear–critical corner joints is presented, including two as–built specimens and one retrofitted using fully–fastened–haunches (FFHR). Bi–axial tests adopted hexagonal protocol which is essentially to apply load in one direction double with respect to the other. Results obtained for as–built condition were included in a database of corner joints tested bi–axially and discussed in the light of the impact of bi–axial load on joint's shear strength. Further, non–linear finite elements were employed to thoroughly evaluate the bi–axial response. Haunch retrofit was capable to reduce both shear stresses and distortion at joint. Experimentally–derived internal forces were used to validate three–dimensional Strut-and-Tie model of the joints. Such design tool is recommended for practice cases adopting FFHR.

Keywords Reinforced concrete · Beam–column joints · Bi–axial · Seismic · Haunch retrofit

1 Introduction

It is a common opinion that corner joints require special attention when assessing the seismic performance of a reinforced concrete (RC) moment resisting frame. For example, according to Priestley (1997): "There is reason to expect that corner joints might represent the critical conditions in building frames because of the bi–axial input, typically difficult reinforcement detailing problems involved in anchoring two orthogonal sets of beam bars in the joint, and the influence of variable axial load. Despite this concern, there are almost no test data available for this type of joint".

Priestley et al. (2007) suggested for new structures to provide separate exterior columns for the orthogonal frames to reduce bi–axial beam input and high variations in column's axial force. In the context of existing RC buildings the issue remains and difficulties might

✉ Marchisella Angelo
angelo.marchisella@polimi.it

Muciaccia Giovanni
giovanni.muciaccia@polimi.it

[1] Department of Civil and Environmental Engineering, Politecnico di Milano, Piazza Leonardo da Vinci, 20133 Milan, Italy

Published online: 18 March 2024

be exacerbated by inadequate joint's shear strength which is caused either by the lack or by the absence of transverse reinforcement (hoops) as frequently observed in post–earthquakes surveys e.g. Dislsiz (2023). As a result, the designer might be forced either to strengthen the joints or to lower their shear demand. The former is typically achieved by adopting external reinforcement which aims to integrate existing hoops, e.g. corner joints reinforced using fiber–reinforced–polymer have been investigated by Engindeniz et al. (2005) and Akguzel and Pampanin (2010a).

Aside from the adoption of global retrofit intervention (e.g. insertion of shear walls) which might reduce the seismic demand in existing members according to Antoniou (2023), reduction of joint's shear demand can be obtained by adopting local retrofit such as haunch retrofit. Such technology has been introduced by Pampanin et al. (2006), who adapted to two–dimensional (2D) RC beam–column joint what was originally conceived, by Yu and Gross (2000), for steel moment resisting frames. Essentially, a change of internal forces (bending moment, shear) is obtained by introducing steel diagonal element (haunch) at beam–column joint. The reduction of joint's shear demand is proportional to haunch's stiffness, although the relationship is not linear. Experimental studies addressing RC haunch retrofit have been mainly focused on 2D exterior joints, as it emerges from literature review in Marchisella and Muciaccia (2023). To the Authors' knowledge, only Chen (2006) considered bi-axially loaded corner joint concluding that haunch stiffness might be reduced by torsional behavior affecting beams.

In this paper, the results of an experimental campaign addressing RC beam–column corner joints (which will be referred throughout this paper by the abbreviation "corner joints" or simply "joints") is presented. Three full–scale joints, with slab, were tested bi–axially at Politecnico di Milano between 2020 and 2021. Joints were unreinforced, i.e. without hoops inside the joint's core. Two specimens were tested as–built and one specimen adopting fully–fastened–haunch–retrofit (FFHR). Tests were carried out without imposing axial load to the column.

Three major aims have prompted the presented study. These are:

(i) To contribute to the discussion on influence of bi–axial condition on joint's shear strength;
(ii) To test bi–axially loaded joints, retrofitted using FFHR;
(iii) To validate three–dimensional Strut-and-Tie model (STM) of bi–axially loaded joints.

Each of these scopes is now examined further.

First, the debate on the influence of bi–axial load on joint's shear strength has not reached a conclusive statement to the point that different provisions are given by design codes or guidelines. For example, EC8 (2004) prescribes that joint's shear verification should be carried out independently in two directions without any strength's reduction. Conversely, ACI (2002) and NZSEE (2017) propose elliptical interaction domain and 30% strength's reduction, respectively. Priestley (1997) proposed (i) To evaluate the shear demand as vectorial summation of two orthogonal shears and (ii) To limit the principal tensile stress evaluated on joint to a value equal to $0.58 \cdot \sqrt{f_c}$, where f_c is the concrete compressive strength. Further, tests made to provide experimental evidence differ on the applied bi–axial load protocol. In this light, the paper presents a systematical collection of test units surveyed from literature. Inspired by Opabola et al. (2020) who investigated the influence of load protocol on bending–shear strength of bi–axially loaded RC columns, an attempt to similar discussion is given for shear–critical joints. In addition, to provide

an improved understanding of mechanical response of bi–axially loaded joints, results obtained using non–linear finite elements models are presented.

Second, FFHR has been originally proposed by Sharma et al. (2014) for 2D joints. Generally, the adoption of direct fastening mitigate the invasiveness with respect to passing rods adopted in the past, e.g. Pampanin et al. (2006). Experimental results on FFHR applied to exterior joints with slab and transverse beam presented in Marchisella et al. (2021) showed that both slab's participation and torsional behavior of transverse beam influence the joint's mechanical response. Based on common perception, bi–axial input loads at joint is supposed to impact as well. Although this aspect has been already claimed by Chen (2006), generalization is hard to pursue because results may be jeopardized by the selected load–protocol and slab's participation. In this light, the presented experimental campaign extends the available experimental data.

Third, prediction of internal forces (e.g. joint's shear demand, haunch's diagonal force) for haunch retrofitted RC joint was presented by Pampanin et al. (2006) upon the definition of β-factor which condenses kinematic compatibility imposed between haunch and concrete elements, i.e. beam and column. Such approach has been questioned by Marchisella and Muciaccia (2023) for haunches which are made with large base plates as for the case of FFHR. Application of STM has been proposed instead and results were compared to FEM models of 2D joints. The extension of such approach to corner joint was mainly inspired by Yun et al. (2018a, b) who applied STM to three–dimensional structures such as pile caps, slab–column joints and beams in torsion. For corner joints loaded bi–axially one major enhancement is required, with respect to 2D joints, that is to adopt three-dimensional grid of struts to model the compressive field which characterizes both membrane response of slab and torsion of beams. Analytically–derived internal forces are compared to experimental ones largely using, for the latter, load conversion of strains measured at steel reinforcement as suggested by Mitchell et al. (2002).

The paper is structured as follows. The second section summarizes both the background of bi–axial load protocols and the state–of–the art of RC beam–column joints tested bi–axially. In the third section both experimental setup and results are described. The main findings are discussed in the fourth section. The last section provides a summary of the work along with the conclusions drawn. Given the space limitations, database of corner joints tested bi–axially is given in an Appendix.

2 Seismic bi–axial input: background

2.1 Bi–axial displacement protocols

According to Rodrigues et al. (2013), conventional displacement protocols cannot be considered as representative of an earthquake, although they compromise the need of bi–axial input with smooth increase of the peak displacements to capture the strength and stiffness degradation. For example, bi–axial tests on RC columns (usually loaded axially) are performed often by imposing a coupled displacement time history at column's tip. Figure 1, shows different bi–axial displacements protocols. For the sake of a general description, the x and y axis are termed as "variable". According to Opabola et al. (2020), the coupling between variables can be quantified using a coupling factor (C.F.) defined as the ratio between the median of all bi–axial vectors in the first quadrant and $\sqrt{2}$, as shown in Fig. 2.

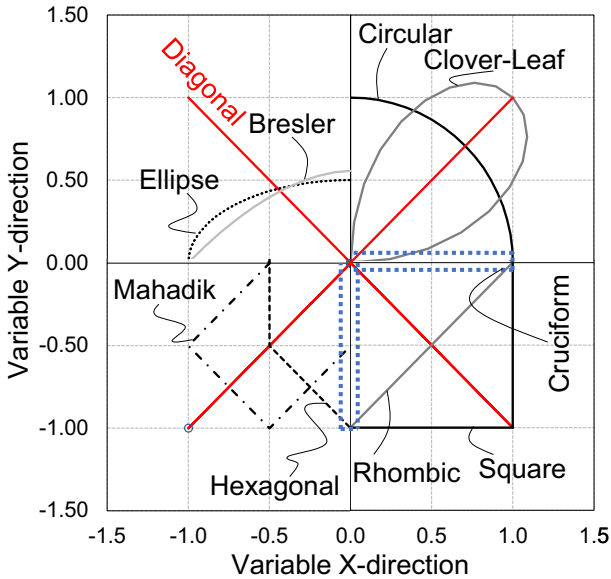

Fig. 1 Bi–axial load protocols. (Notes. One–quarter of the orbital is represented for each case except for the diagonal)

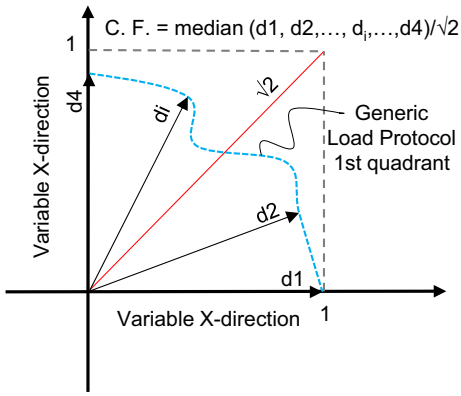

Fig. 2 Coupling factor (C.F.) definition

Consequently, the cruciform and the diagonal path, have zero and unitary C.F., respectively. Other C.F. for different load protocols are listed in Table 1.

Menun (2000a) derived analytically elliptical envelopes for the displacements of N–degrees–of–freedom linear structures characterized by (i) Two major structural directions and (ii) Bi–axial input motion in horizontal direction. Similar bi–axial envelopes were obtained by Menun (2000b), performing linear time–history analysis, for internal forces, e.g. columns' bending moment. In this light, it is the Authors' opinion that shear demand at joint, which is linearly related to internal forces, can be enveloped by ellipses as well. To the scope, an example is presented hereinafter.

Bi–axial shear demand at corner joints of SPEAR frame (tested by Negro et al. 2004) was investigated extending the numerical results presented in Marchisella and Muciaccia (2022). Dynamic response was obtained using time–history analysis. Simultaneous base accelerations were imposed in two horizontal directions. Materials were linear elastic and joints were modeled as rigid according to Birely et al. (2012). Figure 3 shows

Table 1 Coupling factors (C.F.) evaluated for different bi–axial load protocols

Protocol	C.F.
Cruciform	0.000
Hexagonal	0.500
Ellipse	0.560
Rhombic	0.604
Cloverleaf	0.640
Circular	0.707
Mahadik†	0.790
Square	0.790
Diagonal	1.000

† Mahadik and Sharma (2021) proposed a bi–axial load protocol for RC beam–column joints

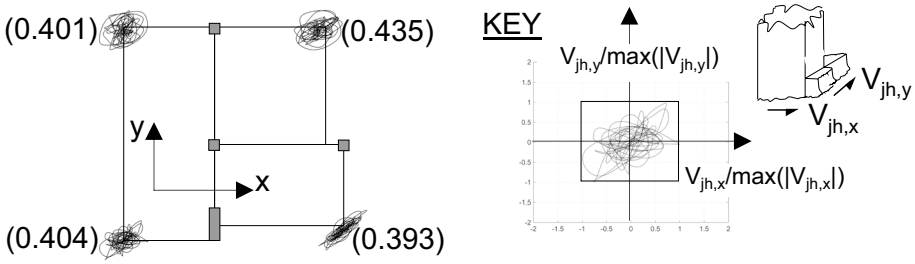

Fig. 3 Numerically–derived joint's shear demand orbitals and evaluated C.F. (in round brackets) for corner joints of the SPEAR frame, tested by Negro et al. (2004)

bi–axial shear orbitals obtained at corner joints of the first story along with their evaluated C.F.(values inside round brackets in the figure). The latter was equal to 0.408 on average. As expected, the orbitals are generally enveloped by ellipses although the result can suffer lack of generality because it was obtained for a single input motion.

2.2 Beam–column joints tested bi–axially

Experimental studies on RC beam–column joints tested bi–axially have been systematically collected in Table 2. Only English literature was surveyed, however the Authors are aware of conspicuous Japaneses investigations on the same subject, e.g. (Nishimura et al. 2014; Sano et al. 2022; Ishizuka and Kitayama 2016).

For the surveyed investigations design was usually based on gravity loads, thus joints were characterized by lack of horizontal reinforcement. Figure 4 shows the typical specimen which represents a corner joint isolated from moment–resisting–frame under shear sway in both planes. In such a case, contra–flexure points are expected to form in the middle of both beams and columns. In most of the surveyed cases, displacement histories were applied at beams' tips, however there were cases where bi–axial protocol was imposed at the top of the column, e.g. tests carried out at Christchurch (New Zealand).

Table 2 Literature survey on RC beam–column joints tested bi–axially

References	Joint-type	Design	Scale	Pr.	Specim.		ρ_{sh}	Var.	Retrof.
Notes		(a)		(b)	(c)		(d)	(e)	(f)
					Uni	Bi	(1/100)		
Burguieres et al. (1980)	Interior	ACI352	1/1	⋄	0	4	0.37	–	–
Leon and Jirsa (1986)	Corner	NA	1/1	† – ⋄	1	13	0.29	ν	–
Kurose et al. (1991)	Corner with Slab	ACI352	1/1	⊔	3	2	0.55	–	–
Chen (2006)	Corner	Gravity	2/3	⊗	1	1	0	–	Haunch
Engindeniz (2008a, b)	Corner with slab	Gravity	1/1	†	0	1	0	–	FRP
Akguzel and Pampanin (2010b)	Corner	Gravity	2/3	⊗	6	4	0/0.09	ν	GFRP
Kam et al. (2010)	Corner with slab	Gravity	2/3	⊗	1	1	0	–	–
Park and Mosalam (2013), Park (2010)	Corner with slab	Gravity	1/1	†	0	4	0	h_c/h_b	–
Hassan and Moehle (2012), Hassan (2011)	Corner with slab	Gravity	1/1	⋄	3	1	0	$\nu, h_c/h_b$	–
Kitayama and Katae (2017)	Corner with slab	AIJ	1/2	⊔	0	2	0.28	ν	–
Hosseini et al. (2018)	Corner	ACI 318	1/1	⊗	0	4	0.47	ν	ECC
Li et al. (2019)	Interior	NA	1/1	NA	0	3	0.19/0.3	ρ_{sh}	–
Han and Lee (2020, 2022)	Corner with slab	ACI 318	1/1	∪	1	2	0/0.20	ρ_{sh}	–
Sano et al. (2022)	Corner	AIJ	1/2	⊔	1	3	0.21/0.47	ν	–

(a) Adopted design method: [Gravity] Gravity–based design; [ACI352; ACI318] Seismic design according to ACI (2002) or ACI (2019); [NA] Not–available. (Note. References were made to the most updated version of the code, however design period may not correspond. Reference to Japanese code AIJ was not found.)

(b) Load Protocol (see also Fig. 1): [⋄] Diagonal; [†]Cruciform; [⊔] Square; [∪] Hexagonal; [⊗] Clover-leaf; [NA] Not–available

(c) Specimens used in experimental campaign: [Uni] Tested uni-axially; [Bi] Tested bi-axially

(d) Hoops ratio

(e) Joint's test variables: [ρ_{sh}] Hoops ratio; [ν] Normalized column axial load; [h_c/h_b] Aspect ratio

(f) Retrofit technique adopted: [GFRP] Glass–fibers–reinforced–polymer; [FRC] Fiber–reinforced–polymer; [ECC] Engineered–cementitiuous–composites

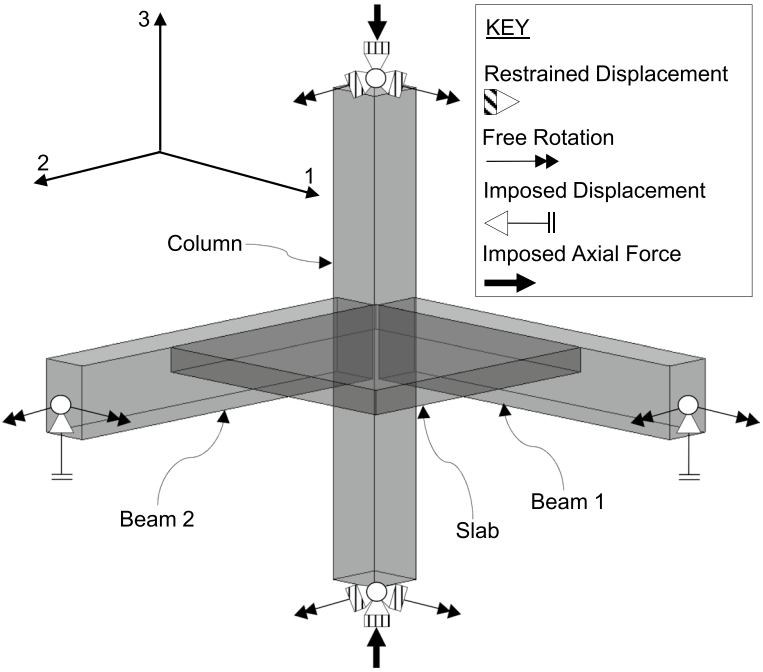

Fig. 4 RC beam–column corner joint

Leon and Jirsa (1986) tested corner joints under uni–axial, cruciform and diagonal displacement protocol. The overall shear capacity was slightly affected by bi–axial input. However, due to the loss of the corner's edge reduction of bending capacity was observed.

Akguzel and Pampanin (2010b) and Kam et al. (2010) tested corner joints using clover–leaf displacement protocol. Bi-directional response resulted in 30 and 60% reduction in the lateral load capacity and energy dissipation, respectively, if compared with uniaxial response. Similar results, considering unreinforced to moderate reinforced beam–column joint were obtained by Han and Lee (2020) using hexagonal displacement protocol. Hassan and Moehle (2012), Park (2010) and Engindeniz (2008a) used cruciform displacement protocol reporting moderate reduction of the joint shear strength.

Different conclusions were obtained by Kurose et al. (1991), using half-square displacement protocol. Bi-directional shear strength was found to be higher than uni-directional if the former is evaluated as the square root of the sum of the squares of shear measured in orthogonal directions at the time of maximum bi-directional response.

Burguieres et al. (1980) tested reinforced joints observing no change in shear strength by increasing the reinforcement. However, the inelastic deformation ascribable to the column and to the beam showed significant changes. Same conclusions were reported by Kitayama and Katae (2017).

Quintana-Gallo et al. (2021) tested scaled three-dimensional frame on shaking table. Corner joints were characterized by severe diagonal cracking and crushing of the joint core.

Numerical comparison between uni–axially and bi–axially loaded joints have been performed by Alaee et al. (2015) showing (i) Larger energy dissipation for the former and (ii) Non significant strength differences. Tonidis and Sharma (2021) showed numerically the

beneficial effect of the spandrel beam, due to joint confinement, when corner joint is tested uni–axially. Mahadik and Sharma (2021) discussed the suitability of bi–axial load protocols, applied to shear critical beam–column joint. The effect on shear resistance, considering different coupled shear demand, was studied through non–linear finite elements (brick elements) under static load. The selected benchmark was the corner joint tested by Park (2010). The smallest shear resistance was obtained having imposed the same displacement to the beams either in-phase or out-of-phase. Results were placed in the context of combination rules for seismic responses. The adoption of either 100:40 or 100:50 rule was reported as more reliable. A displacement protocol was then developed having the proportion of displacements, acting in two framing directions, in a range of 100:0 to 100:50 or 0:100 to 50:100. To Authors' opinion, such discussion cannot be sustained conclusively. In fact, combination rules have resulted in contradictory performance when compared with combined peak analysis (an example was reported by Salami et al. 2021), knowing that individual responses maxima or minima do not occur, normally, at same time as remarked by Menun (2000a). For instance, Newmark (1975) defined the combination rules as generally conservative although it has been recently contradicted by Wang et al. (2019).

3 Experimental investigation

3.1 Specimens' details

Three corner joints were built in 2020 and tested in 2021 at Material Testing Laboratory of Politecnico di Milano. The nomenclature of the specimens is given in Table 3.

Figure 5 shows the sub–assemblage's geometry and the reinforcement layout. The specimen had (i) 300 mm wide by 470 mm deep beams and (ii) Square column with 350 × 350 mm cross-section. The slab was 180 mm thick. The slab's reinforcement (two layers ϕ12 with 150 mm spacing) extended to the back of the beam with bent anchorage. The beam's longitudinal bars were anchored inside the joint with 90° bent. Large diameter (26 mm) reinforcement was used for beams to promote joint's shear failure without yielding of steel. Net concrete cover was equal to 30 mm. Reinforcement cage was assembled before and inserted in the formwork as shown in Fig. 6a.

Casting of specimens (see Fig. 6b) was two–phases. First, concrete was poured in the formwork up to the level of slab's extrados. One day after, the remaining upper part of the column was completed. The resulting specimen's self–weight was approximately equal

Table 3 Tested specimens

Code	Type	f_{cc} (MPa)	f_{ct} (MPa)	Notes
CJ01	As-Built	36.5	3.6	(a)
CJ02	As-Built	36.5	3.6	–
CJ03	Retrofit	36.5	3.6	(b)

f_{cc} is the cubic compressive strength; f_{ct} is the tensile strength derived from four–point bending tests

(a) Trial tests were performed to tune the test apparatus

(b) Double haunch retrofit, for beam–column joint was adopted only for the primary beam, viz. Beam 1 according to the test protocol shown in Fig. 1

Table 4 Yielding stress of reinforcement steel

$\phi 10$	$\phi 12$	$\phi 20$	$\phi 22$	$\phi 26$
519(610)	530(646)	520(629)	534(648)	532(642)

Values are in MPa. Ultimate strength is given inside the round brackets

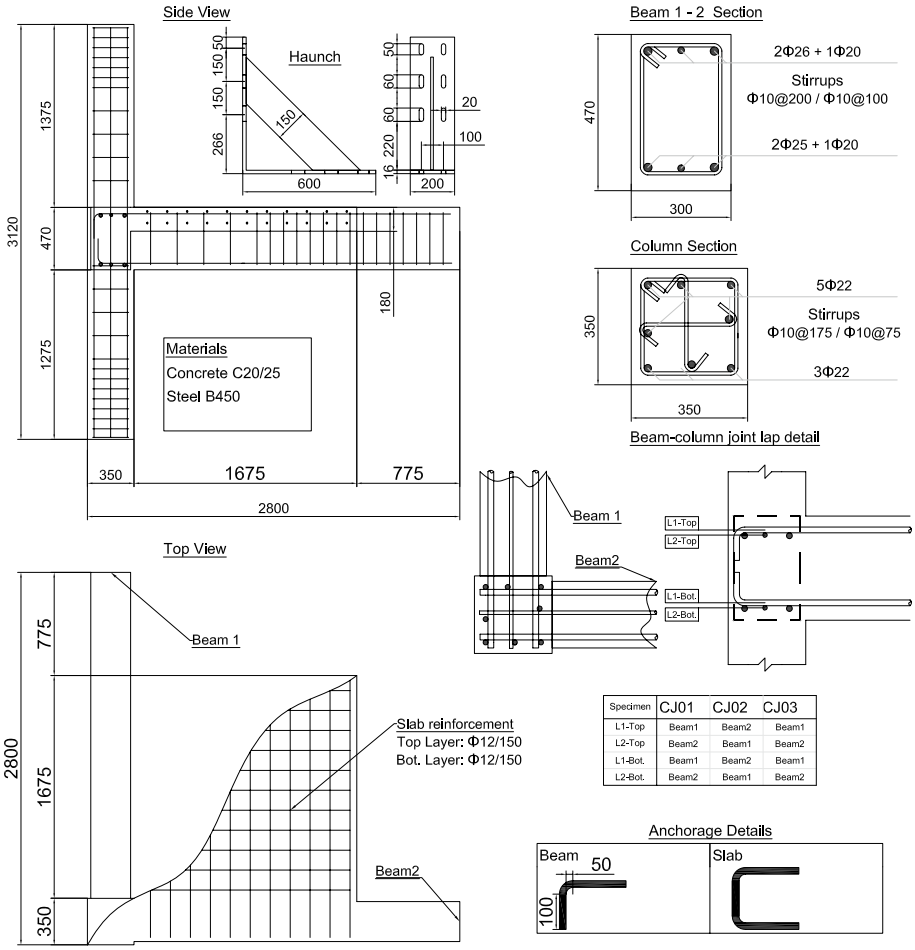

Specimen	CJ01	CJ02	CJ03
L1-Top	Beam1	Beam2	Beam1
L2-Top	Beam2	Beam1	Beam2
L1-Bot.	Beam1	Beam2	Beam1
L2-Bot.	Beam2	Beam1	Beam2

Fig. 5 Corner joint specimen: geometry and reinforcement layout. (Notes. Dimensions are given in millimeters)

to 4000 kg. Nominal concrete class was C20/25 according to EC2 (2004), which had a mean value of cubic compressive strength equal to 36.5 MPa. According to Neville (1996), concrete tensile strength was assumed equal to $\frac{3}{4}$ of the flexural strength obtained from four–points bending tests having a mean value equal to 3.6 MPa. Reinforcement steel was B450C class (f_{yk} = 450 MPa). The mean values of yielding strength, for different diameters, are reported in Table 4.

Fig. 6 Corner joint specimen: **a** formworks and reinforcement cage; **b** casting operation. (Note. The Reader is referred to the color version of this figure)

Test setup is schematically represented in Fig. 7 and a photographic report is given in Fig. 8. The specimen was tested with column standing vertically. Two swivels were connected to the column's end sections using collars tightened with threaded bars. Restraints to vertical translations were applied both at the top and at bottom of the column. Specifically, a grid of beams connected to the strong floor was used for the bottom swivel. Top one was pinned to a reaction frame. Such configuration, as shown in Fig. 9, implies simultaneous tension and compression in the column when both self–weight and seismic shears are acting. To increase the column's tensile strength, additional post–installed steel bars were installed at the end sections. Horizontal sliding of the bottom swivel was prevented using contrasting plates (see Fig. 8d). The top swivel was restrained horizontally by using eight steel wires (see Fig. 8e). The rigid-body rotation of the slab plane was restrained

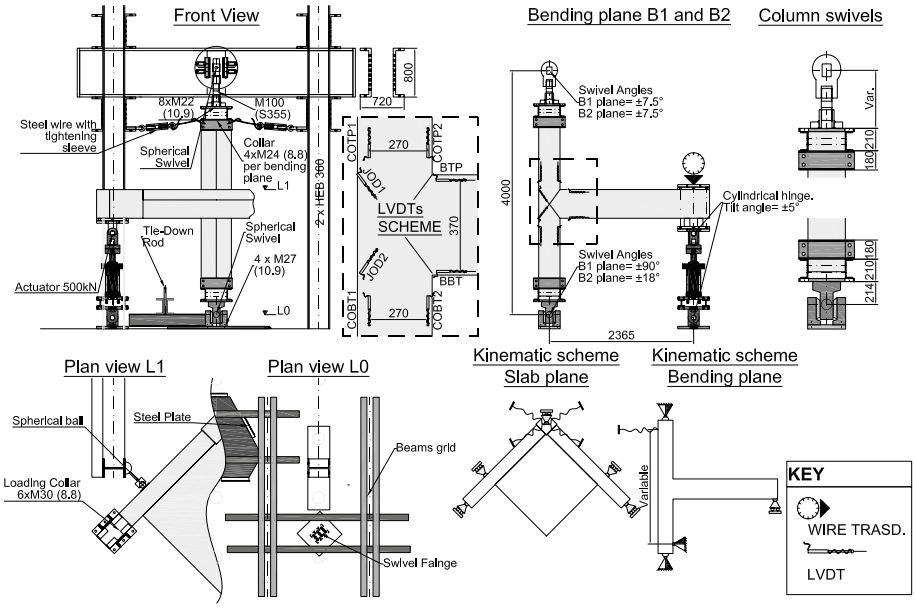

Fig. 7 Experimental test setup used for corner joints. (Notes. Dimensions are given in millimeters)

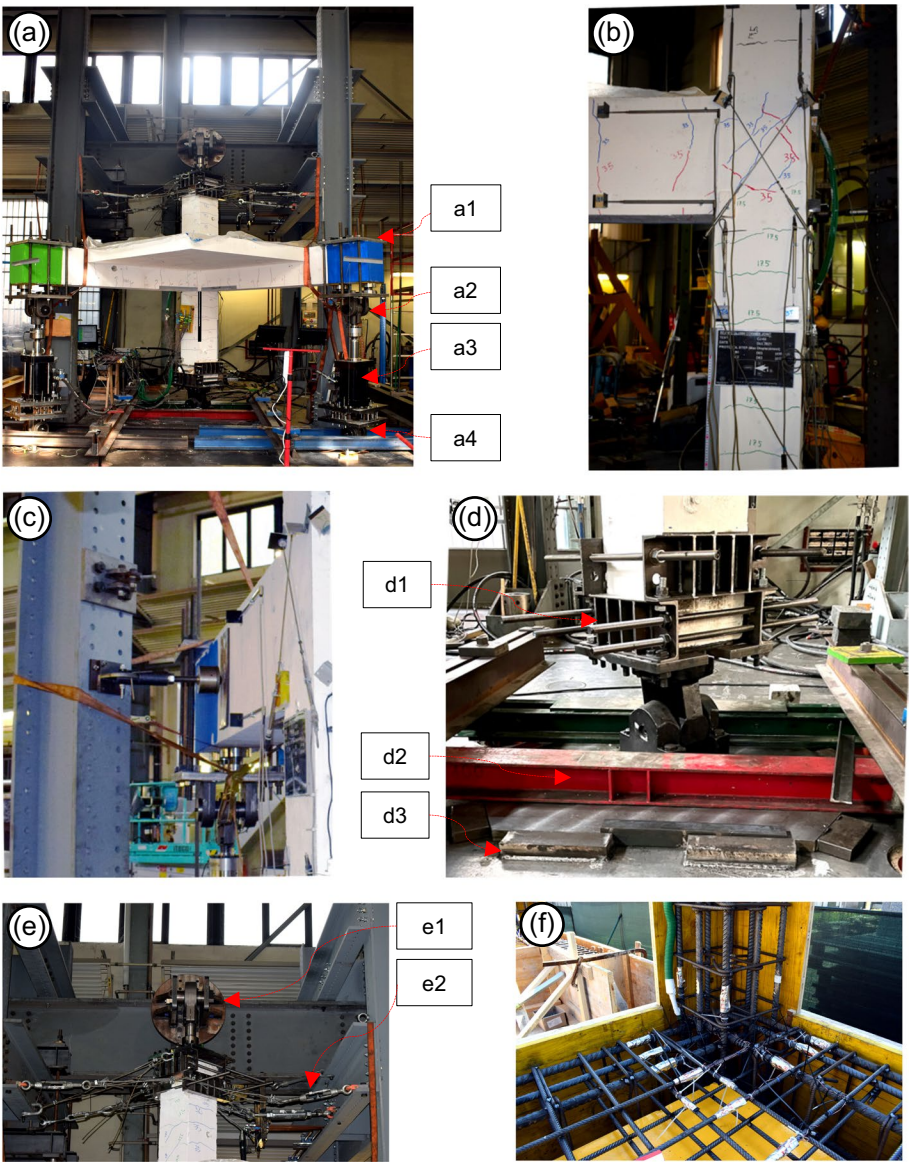

Fig. 8 Photographic report of experimental test setup used for corner joints: **a** front view; **b** linear–displacement–transducers at one side; **c** restraint to rigid–body rotation; **d** bottom swivel; **e** top swivel; **f** strain gauges glued onto reinforcement steel at column face. (Notes. (a1) Loading collar. (a2) Cylindrical hinge with allowed torsional tilt. (a3) Hydraulic cylinder 500 kN load capacity, 250 mm maximum displacement. (a4) Cylindrical hinge with allowed torsional tilt. (d1) Restraint collar. (d2) Uplift restraint. (d3) Sliding restraint. (e1) Cylindrical hinge with allowed torsional tilt. (e2) Rope tightened with sleeves. The Reader is referred to the color version of this figure)

by rollers (see Fig. 8c). At the beams loading point, two 500 kN hydraulic actuators were pinned to loading collars. To guarantee torsional rotation, the pin allowed tilt angles up to five degrees.

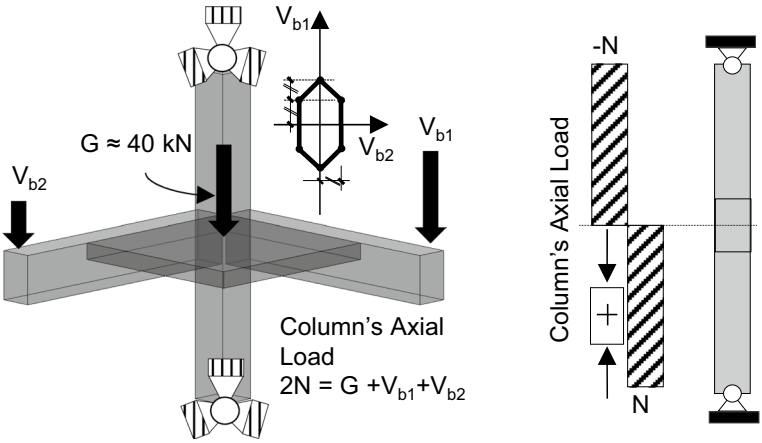

Fig. 9 Axial force in column

The resulting kinematic schemes both in the slab's plane and in the bending planes are shown in Fig. 7. The distance between horizontal restraints, in the bending plane, was variable because of the collars' eccentricities. Furthermore, the restraint at the top is represented as a "spider" of elastic springs. In fact, although the ropes were tightened at the beginning of the test, their deformability cannot be totally neglected. To overcome such issue, the equivalent drift was experimentally–derived by considering only local rotations of beams and column and joint's distortion as explained in the following paragraph 3.2.

Bi–axial tests were performed using hexagonal displacements protocol according to ACI (2015). Figure 10 shows the displacements' time histories in two directions as well as the elementary load–cycle in the bi–axial plane. The primary direction and secondary are hereinafter termed as "B1" and "B2", respectively. When the displacement of B1 is at its maximum, the displacement at B2 is zero. The post–peak transition along B1 from the peak displacement to half of the peak displacement is accompanied by an increase of displacement up to 50% of B2. Hence, the maximum displacement applied simultaneously in both B1 and B2 corresponds to half of the level of maximum displacement.

3.2 Local responses: rotations, joint's distortion, joint's shear stress

Drift was defined according to Fig. 11 where it shown the deformed shape of beam-column joint emphasizing the contribution to deformation of beam's and column's local rotations and joint's distortion. According to Uzumeri (1977), beam-column joint specimen in which the load is applied to the beam (specimen 1) and the column stands vertically is equivalent to the specimen in which the load is applied to the top section of the column (specimen 2) by considering its rotated configuration. By comparing the two configurations, it is worth to note specimen 1 cannot replicate possible P-δ effects. However, according to Ong (2022), such effect is usually negligible for the sub-assemblage both because the level of axial load is generally moderate and column is usually characterized by low slenderness. Drift is rigorously defined for specimen 2 as it follows:

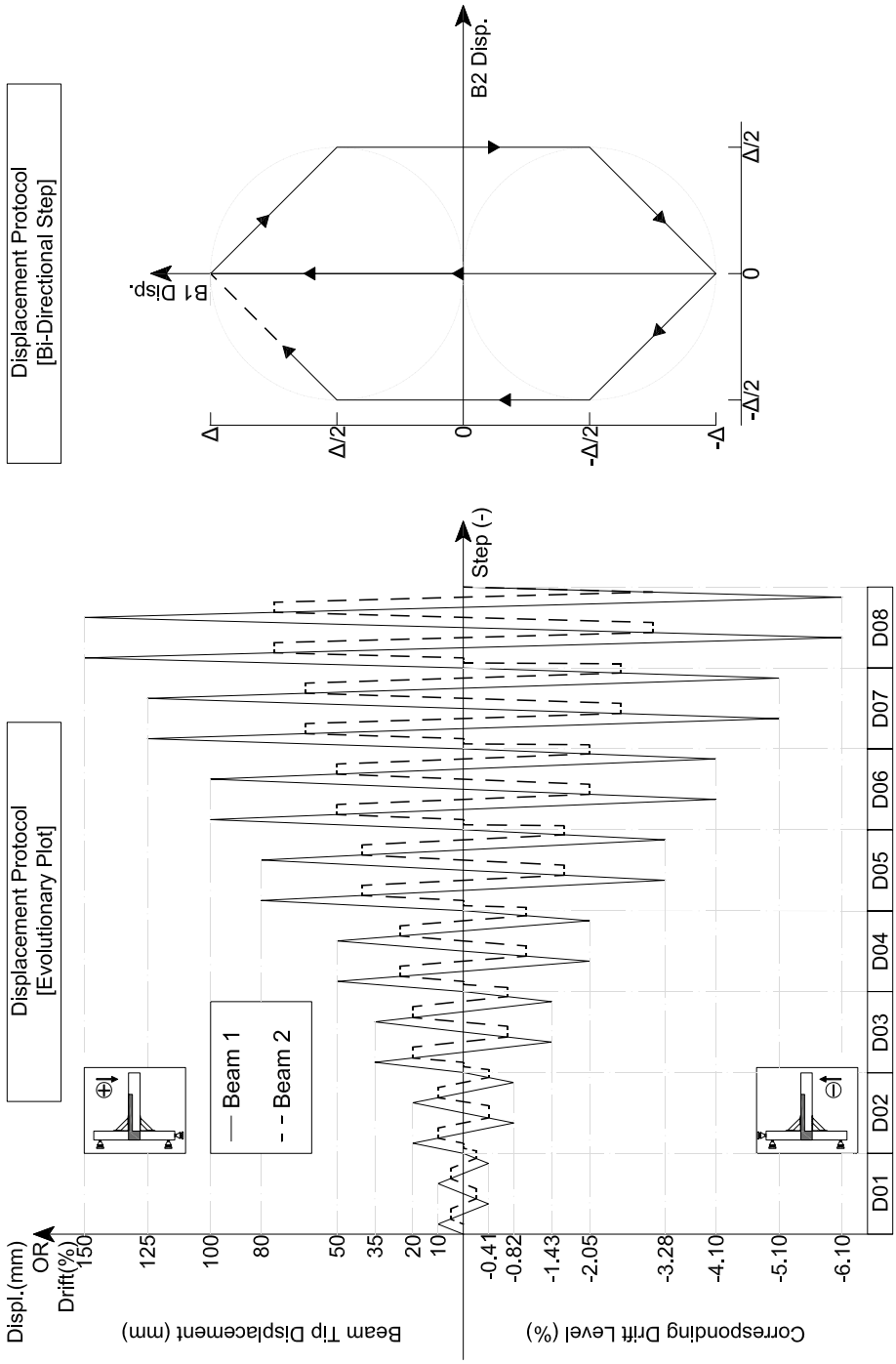

Fig. 10 Hexagonal bi–axial load protocol

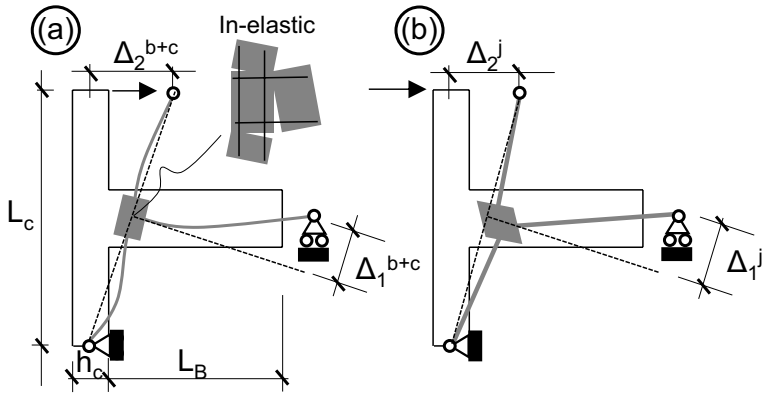

Fig. 11 Definition of drift for beam–column joint: **a** beam's and column's contribution; **b** joint's contribution

$$\delta_2 = \frac{\Delta_2^{b+c} + \Delta_2^{j}}{L_c} \tag{1}$$

where L_c is the column's height and Δ_1^{b+c}, Δ_1^{j} are the displacements given by elastic and inelastic deformation of the beam, column and joint respectively. It is worth to mention that δ_2 corresponds to the chord rotation of the column. Equivalently, drift for specimen 1 can be written as the chord rotation of the beam:

$$\delta_1 = \frac{\Delta_2^{b+c} + \Delta_2^{j}}{L_b + h_c/2} \tag{2}$$

where L_b is the column's height. According to Fardis (2009), compatibility of chord rotations (i.e. $\Delta_1 = \Delta_2$) can be assumed when plastic hinge is expected to form in the beam. Such assumption is usually extended for the case of joint shear failure.

According to Bonacci and Pantazopoulou (1993), when inelastic behavior is predominant (e.g. plastic hinge of the beam, joint's failure): Δ_1^{b+c} is proportional to the rotations measured in the vicinity of the joint for both beam and column; Δ_1^{j} is proportional to the joint's distortion.

To obtain local rotations as well as joint's shear distortion, linear displacements transducers were attached to the specimen as shown in Fig. 8b. The measured displacements were converted into equivalent rotations according to Fig. 12. In particular, the joint's distortion was experimentally–derived as it follows:

$$\gamma_j = [\delta_{1,d} - \delta_{2,d}] \frac{\sqrt{h_b^2 + H_c^2}}{2 h_b h_c} \tag{3}$$

where $\delta_{1,d}$ and $\delta_{2,d}$ are the measured displacements of diagonals, h_b and h_c are the beam's and column's sides, respectively.

The experimentally–derived beam's rotation is:

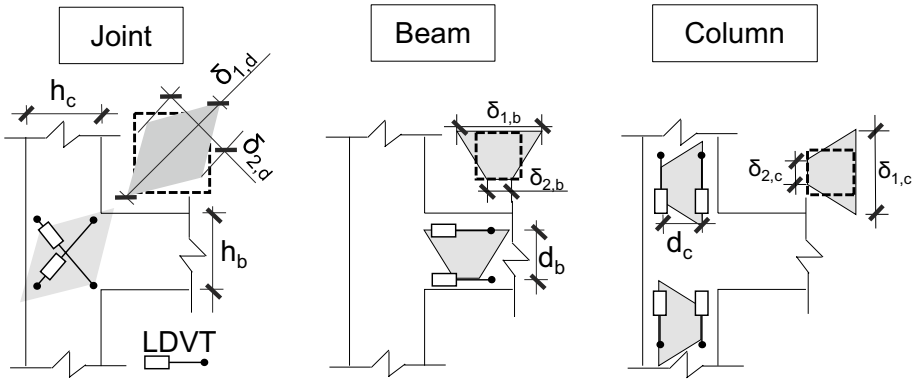

Fig. 12 Joint's distortion, beam's and column's rotations measured using linear displacements transducers (LVDT)

$$\theta_b = \frac{\delta_{1,b} - \delta_{2,b}}{d_b} \tag{4}$$

where $\delta_{1,b}$ and $\delta_{2,b}$ are the measured displacements of top and bottom fibers, d_b is the distance between the measuring devices.

The experimentally–derived column's rotation at top of the joint (similarly for bottom) is:

$$\theta_c = \frac{\delta_{1,c} - \delta_{2,c}}{d_c} \tag{5}$$

where $\delta_{1,c}$ and $\delta_{2,c}$ are the measured displacements of left and right fibers, d_c is the distance between the measuring devices.

Besides, average joint's shear stress has been experimentally–derived by applying the following equation:

$$v_j = \frac{F_L - V_b \cdot L_b/H_c}{A_j} \tag{6}$$

where F_L is the force developed at beam's longitudinal bar derived from conversion of strain measurement, V_b is the load applied at beam, A_j is the joint's area equal, for the sake of simplicity, to the column's area. According to Priestley (1997), state of stress at joint should be described by principal stresses (p_t, p_c) defined as it follows:

$$p_t = \frac{f_a}{2} - \sqrt{\left(\frac{f_a}{2}\right)^2 + v_j^2} \tag{7}$$

$$p_c = \frac{f_a}{2} + \sqrt{\left(\frac{f_a}{2}\right)^2 + v_j^2} \tag{8}$$

where $f_a = P/A_c$ and is the column's axial stress at joint for P is positive in compression. In the presented experimental campaign, the magnitude of f_a was markedly lower with

respect to v_j as much as such the joint was almost characterized by pure shear stress state ($p_t = p_c = v_j$).

3.3 Assessment of joint's seismic performances

Beam–column joints specimens were designed by considering the strength hierarchy of the following failure mechanisms: (i) Shear–bending failure for beam and column; (ii) Anchorage failure of beam's reinforcement bars; (iii) Joint's shear failure. The latter was dominant for as–built condition whereas haunch retrofit was adopted to promote flexural failure at beam.

For all the considered mechanisms, analytically–derived strengths and demands are reported in Table 5. Mean values of material parameters were used. Both shear and flexural strengths were derived from freeware software Response–2000 developed by Bentz (2000) (available at https://www.hadrianworks.com/, accessed on March 2023) where, sectional analysis for flexure is based on Popovics (1973) stress–strain relationship for concrete and elastic–plastic hardening for steel reinforcement. Shear resistant model is implemented, in the software, according to Vecchio and Collins (1986). Only minima shear strengths are reported among the adopted stirrups' spacing. For the beam, an equivalent L–shaped cross–section was assumed to take into account slab's participation.

Joint's shear strength was evaluated according to ASCE (2017) guideline, which includes specific provisions for corner joints.

Anchorage of beam's longitudinal reinforcement at joint was verified according to the draft of new (Fib 2022) Model Code. It is worth to mention that available bond lengths (l_b) as well as the reinforcement's stress (σ_s) vary between the as–built and retrofit case. The former was characterized by l_b equal to the column's width minus the concrete cover (i.e. 325 mm) and σ_s almost equal to 250 MPa corresponding to joint's shear failure without yielding of reinforcement. For the retrofit case, beam hinging ($\sigma_s = f_y = 530$ MPa) was expected at a distance equal to 600 mm from the column's face thus the available bond length was 925 mm.

Column's axial load was not actively controlled in tests. As a results, column was characterized by negligible axial stress if compared to v_j. Reliability of such assumption was investigated by considering the building prototype in Fig. 13a. Lateral response, under seismic load, is supposed to be bi–axial assuming hexagonal orbital for base shears (V1 and V2). For the sake of simplicity, design point is assumed at V1's peak that is simultaneous to V2 equal to zero. In such a case, the largest magnitude of internal forces is expected.

Assessment is presented graphically in Fig. 13b which shows the Moment–Axial domain (M–N) according to Pampanin et al. (2007). Demand curves were obtained considering the internal forces at joint when building is subjected to inelastic lateral response as outlined in Priestley et al. (2007). For the sake of simplicity, the formation of columns' hinges at base and joints' shear failure at first floor was assumed. Capacity curves (converted to equivalent moment at column–face) are evaluated by imposing limit states for beam, column and joint. For example, joint's cracking limit is obtained both according to Priestley (1997) which recognizes the influence of axial force and ASCE (2017). For the sake of completeness, the figure includes demands characterizing experimental tests where axial force is simply related to bending moment at column–face by equilibrium considerations as con be inferred from Fig. 9. By intersecting demand and capacities curve in M–N domain, joint's failure precedes both beam's and column's yielding. Nonetheless, such sequence of events does not vary for values of normalized column's axial load between

Table 5 Predicted strengths and demands for beam–column joints specimens

			Strength	Predicted demand					
				As-Built[a]		Retrofit			
						STM[b]		β[c]	
			R_d	S_d	$-(R_d > S_s)$	S_d	$-(R_d > S_s)$	S_d	$-(R_d > S_s)$
Concrete material									
Compr.[d]	f_c	(MPa)	30.3	–	–	–	–	–	-
Tens.[d]	f_{ct}	(MPa)	3.6	–	–	–	–	–	–
Column									
Height	H_c	(m)	2.5	–	–	–	–		
Shear	V_c	(kN)	395	78	✓	180	✓	180	✓
Bending	M_c	(kN·m)	228	100	✓	56	✓	56	✓
Beam									
Net Span	L_b	(m)	2.2	–	–	–	–		
Shear	V_b	(kN)	564	89	✓	204	✓	204	✓
Bending[e]	M_b	(kN·m)	387(327)	195	✓	327	✗	327	✗
Joint									
Shear[f]	v_j	$(\sqrt{f_c})$	0.66	0.66	✗	0.60	✓	0.56	✓
Anchorage[g]	l_b/Φ	(–)	12.5/35.6	8.7	✓	32.3	✓	32.3	✓
Haunch									
Length	L_h	(m)	0.6	–	–	–	–	–	
Axial	F_h	(kN)	619	–	–	253	✓	377	✓
Anchors	N_{anch}	(kN)	252	–	–	179	✓	267	✗
Failure mode[h]									
				JS		BF		BF/AN	

(a) Internal forces were evaluated from statically–determinate solution of beam–column sub–assemblage when the beam is loaded by a tip force, i.e. V_b

(b) Internal forces were evaluated from Strut-and-Tie model developed by the Authors of this paper

(c) Internal forces were evaluated according to β-factor theory developed by Pampanin et al. (2006)

(d) f_c is the cylindrical compressive strength of concrete. f_{ct} is the tensile strength of concrete

(e) () indicates sagging bending moment

(f) v_j strength is evaluated according to ASCE (2017)

(g) l_b/Φ is the bond length–to–diameter ratio

(h) *JS* Joint's shear failure; *BF* Beam's flexural failure; *AN* Anchorage failure

− 0.2 (tension) to 0.3 (compression). To summarize, given the strength hierarchy characterizing the as–built specimen's, joint's shear failure was the weakest mechanism. Although experimental M–N demand at joint differ from the one obtained for building prototype, in both cases the sequence of failure events is not critically influenced by column's axial load.

3.4 Design of haunch retrofit

In retrofitted specimen, double haunch was applied in primary beam's plane. The other plane remained as-built. Such assumption was inspired by an ideal design case where

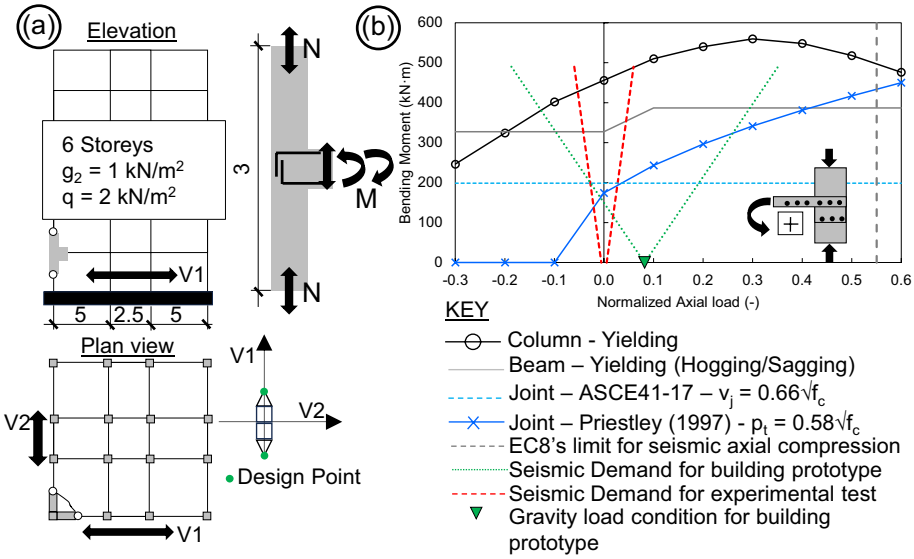

Fig. 13 Joint's performances for as–built condition: **a** building prototype; **b** M–N domain. (Note. Dimensions are given in meters)

only primary direction may be seismic deficient, whereas the secondary may be part of dual system in which shear wall is the leading element. In this case, drift demand is expected to be larger for primary direction than secondary, as stated by Miranda (1999).

Haunch element was made of three steel plates welded together with a thickness of 16 mm. The steel grade was S275 (f_{yk} = 275 MPa). To fasten the haunch to concrete, bonded anchors with 300 mm embedment depth were used for the column, whereas passing rods were adopted for the beam. Anchors were spaced at a distance of 150 and 100 mm along the long and the short side, respectively. The holes were slotted to overcome the interference of rebars during drilling operations.

Haunch retrofit was designed such that, when plastic hinge forms in the beam, both steel plates remain elastic and anchorage failure is prevented. Internal forces, e.g. axial force in the diagonal plate, joint's shear demand were evaluated adopting STM as it is discussed subsequently in Sect. 4.

For the sake of comparison, β-factor approach (according to Pampanin et al. 2006) was adopted as well. Details are given in Table 6. It is worth mentioning that β-factor was evaluated in two ways: (i) Neglecting column's deformability but with a reduced beam's flexural stiffness (EJ_{beam}); (ii) Considering column's deformability but with gross stiffness for beam and column as suggested by Pampanin et al. (2006). To the Authors' opinion the second assumption deviates, somehow, from observed experimental behavior. In fact, since plastic hinge is expected to form in the beam, EJ_{beam} should be evaluated for the cracked cross-section, e.g. either as a fraction of the gross EJ_{beam} (for example 0.3 according to ASCE 2017) or as the ratio between bending moment and curvature at yielding (M_y/Φ_y). Conversely, the column contributes to deformation of the sub–assemblage either with gross stiffness or with cracked one but possibly increased by the presence of axial force according to Elwood (2010). Nevertheless, differences for

Table 6 Evaluated β-factor according to Pampanin et al. (2006)

	Hogging	Sagging	
	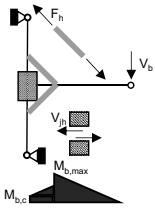	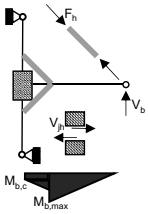	
f_c	30.3		(MPa)
f_y	532		(MPa)
E_c	30678		(MPa)
M_y	387	327	(kN·m)
Φ_y	8.96	7.44	(rad/km)
$EJ_{b,gross}$	8.0E+13		(N·mm^2)
M_y/Φ_y	4.3E+13	4.4E+13	(N·mm^2)
$\beta^{(a)}$	2.63	2.61	(–)
$\beta_{th}^{(a)}$	2.89		(–)
$M_{b,c}/M_{b,max}$	0.27	0.28	(–)
	0.17		(–)
V_{jh}/V_b	1.85	1.87	(–)
	1.58		(–)
F_h/V_b	0.93	0.92	(–)
	1.02		(–)

(a) β-factor has been evaluated neglecting column's deformability but with reduced flexural stiffness of the beam, i.e. M_y/Φ_y. β_{th} has been evaluated considering column's deformability but employing gross flexural stiffness both for beam and column

the two abovementioned approaches are generally mitigated as EJ_{beam} reaches the value M_y/Φ_y.

By comparing internal forces predicted by both STM and β-factor in Table 5, similar results with respect to Marchisella and Muciaccia (2023) are obtained, i.e. β-factor approach predicts lower shear demand whereas the haunch force increases. As a result, retrofitted specimen designed according to β-factor approach would have fail because of anchorage break–out but this has been not observed experimentally as it is presented in the paragraph 3.6. Besides, a comparison between experimentally–derived internal forces and predicted ones is given in the Sect. 4.3.

3.5 Results for as–built specimens

Specimen CJ01 was mainly used to tune the test setup, the result suffered lack of the torsional restraints in the slab's plane (see Fig. 7c) which were introduced afterward. For those reasons results are not presented here.

Results of Specimen CJ02 are shown in Fig. 14a–b. Load–displacement plots are distinguished for B1 (the main beam according to the load protocol described in Sect. 3.1) and B2 (the secondary beam). Crack pattern at the joint is shown Fig. 19a–b.

Crack at column's cold joint opened at the very beginning of the test. Flexural hairline cracks appeared at the location of the beam stirrups and at column–face from initial stages, contemporary joint diagonal cracks started to form. They continued to develop in the form of X-pattern and spread towards the perimeter of the joint. Slight differences in load levels have been observed between hogging and sagging behavior. Joint's panel integrity was compromised after having reached almost 100 kN load level in both

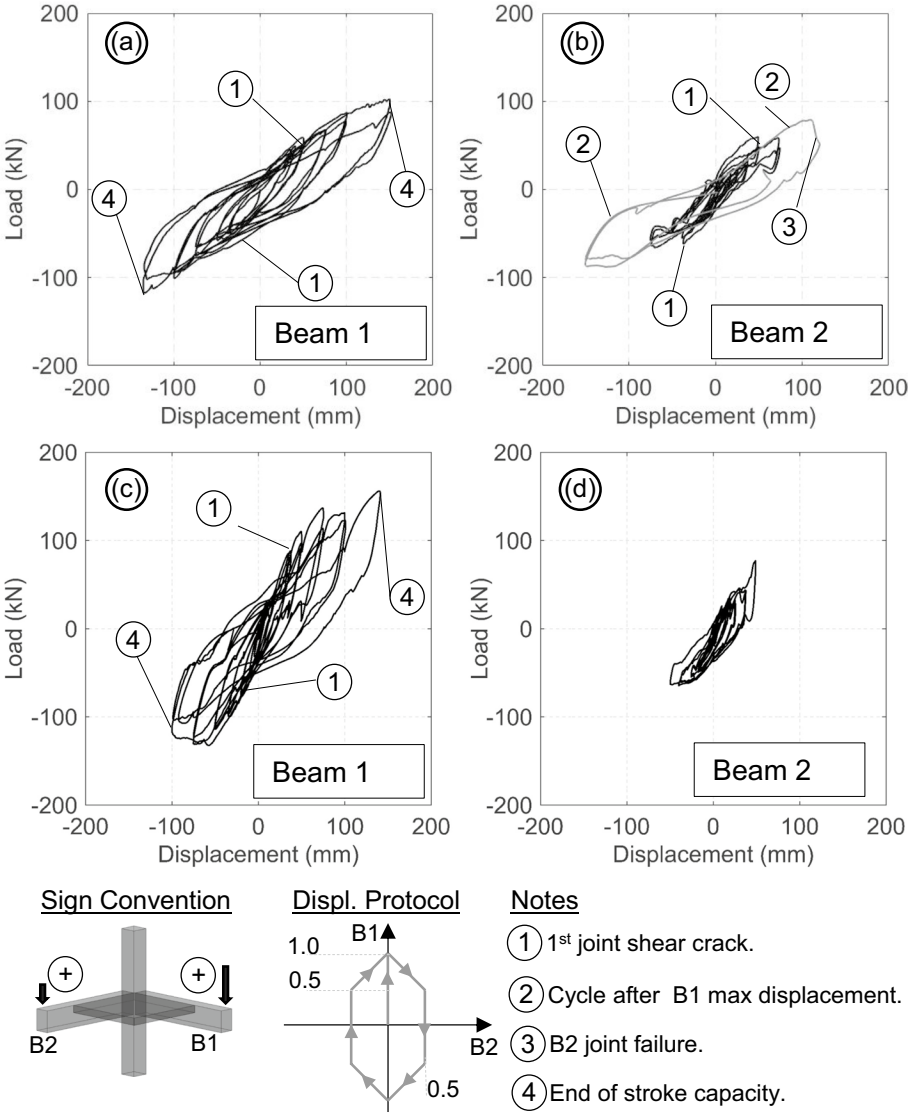

Fig. 14 Tests' results: load–displacement curves for (**a**–**b**) specimen CJ02 and (**c**–**d**) specimen CJ03

direction for B1. Complete detachment of the corner edge was observed. Longitudinal reinforcement of the column were visible at the end of the test as well as the bent anchorages of the B1 longitudinal reinforcement. The test was concluded having reached the maximum available stroke for the hydraulic cylinders. A final monotonic test in B2 direction was carried out and joint's failure was observed at a load level almost equal to 79 kN. After a sudden load drop, the joint panel integrity at B2 side was compromised. Although the longitudinal reinforcement of the column remained completely exposed, its buckling was not observed.

Figure 15 shows the strains measured in the beam's longitudinal rebars at the column face. The reported values were sampled at the first cycle of each displacement steps. For the sake of synthesis, sampling is made considering half-cycle, e.g. bottom layer strain is sampled when the applied load gave sagging behavior. Strains did not reach the yielding threshold assumed equal to 2650 μ-strain. Slab's participation was confirmed being slab's strains comparable to the ones of the beams. Strains measured on B2 (when unloaded) for the peak load stages are represented in Fig. 16. It is worth noting that

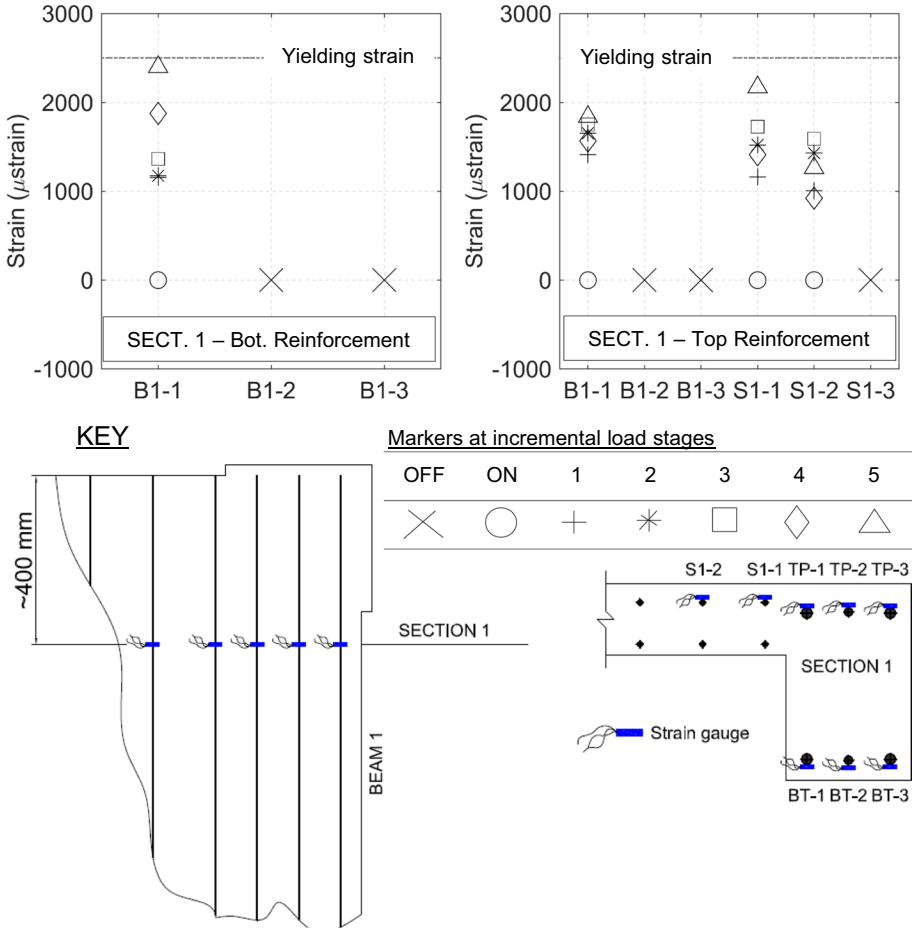

Fig. 15 Test's results: strains measured at B1 of specimen CJ02 when B2 was unloaded

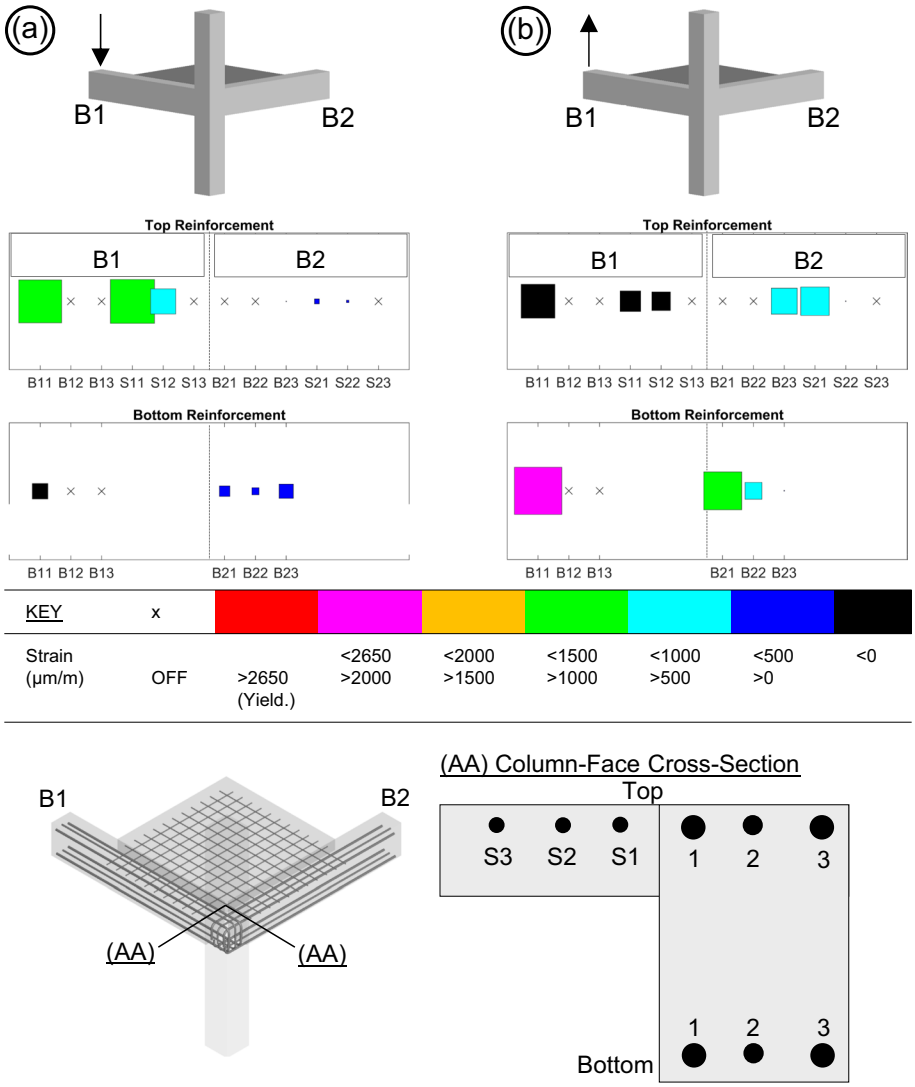

Fig. 16 Test's results: strains measured at B1 and B2 of specimen CJ02, when B2 was unloaded, for two peak load stages, i.e. **a** hogging and **b** sagging. (Notes. The size of squares is proportional to the strains' magnitude. The Reader is referred to the color version of this figure)

steel reinforcement in B2 was activated although the beam was unloaded. Such evidence most probably resulted from torsional response.

Figure 17 shows the experimentally-derived contributions to drift obtained for specimen CJ02. In particular, the contributions due to joint, beam and column to drift were evaluated as explained in paragraph 3.2. It is worth to mention that the sum of the three contribution is lower than the imposed drift confirming the lack of stiffness of the restraints.

The previously described damage state at joint, as well as the experimentally–derived joint's stresses–to–distortion curves of Fig. 18a–b, proved that joint's failure was reached.

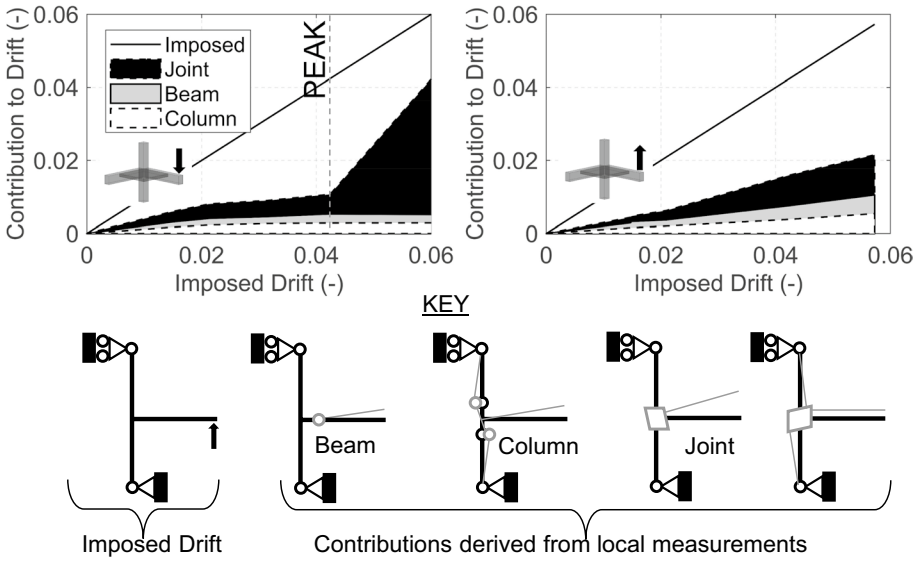

Fig. 17 Tests' results: experimentally–derived drift for specimen CJ02

In fact, considering hogging load direction peak shear stress was comparable to ASCE (2017) reference value, i.e. $0.66\sqrt{f_c}$. Subsequent cycle after peak was characterized by abrupt strength's reduction and large increase of shear distortion. Finally, a reduced joint's deformation capacity emerges if experimental results are compared with degradation curve according to Priestley (1997).

3.6 Results for retrofitted specimen

Specimen CJ03 was retrofitted using haunches at B1 side and tested bi–axially. Load–displacement curves and damage pattern at joint are shown in Fig. 14c–d. and Fig. 19c–d, respectively.

Considering B1 plane, joint's shear cracks were significantly reduced with respect to CJ02. Moreover, increase of the stiffness and load carrying–capacity were observed as well. Haunch's diagonal plate remained in elastic regime. Anchorage to concrete behaved satisfactorily both at the beam and at the column side. The test stopped having reached the maximum available stroke capacity. Both shear distortions and stresses at joint were significantly reduced if compared with CJ02, as shown in Fig. 18c–d.

At B2 side, the behavior was almost linear–elastic with moderate crack pattern at joint, as shown in Fig. 19d.

Figure 20 shows the strains measured at two different cross–sections of B1, i.e. column–face (Sect. 1) and haunch's end (Sect. 2). Strains' reduction is recognized passing from Sect. 1 to Sect. 2 both for hogging and sagging moment. Slab's participation is observed as well. None of the samples have reached the yielding strain. As previously mentioned, the full development of the plastic hinge could not be reached due to the stroke's limitation of the hydraulic cylinders.

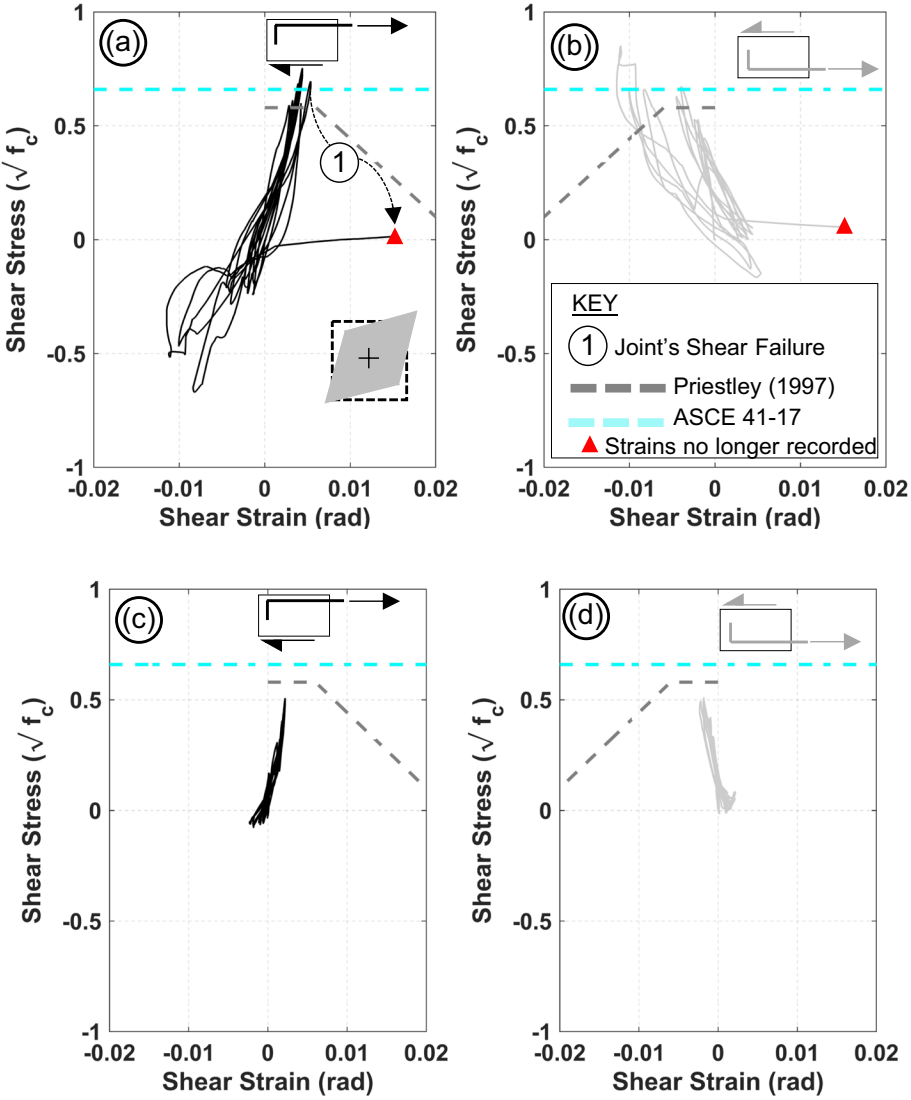

Fig. 18 Experimentally–derived joint's stress–to–distortion: specimen CJ02, **a** hogging and **b** sagging; specimen CJ03, **c** hogging and **d** sagging. (Notes. Joint's shear stresses and distortions were derived using Eqs. (6) and (3), respectively. The Reader is referred to the color version of this figure)

Figure 21 compares the shear–flexural crack pattern obtained in CJ02 and CJ03 for a portion of B1 which extends almost 120 ms from the column–face. Pictures were taken at the end of tests. Inverted shear cracks were observed in CJ03.

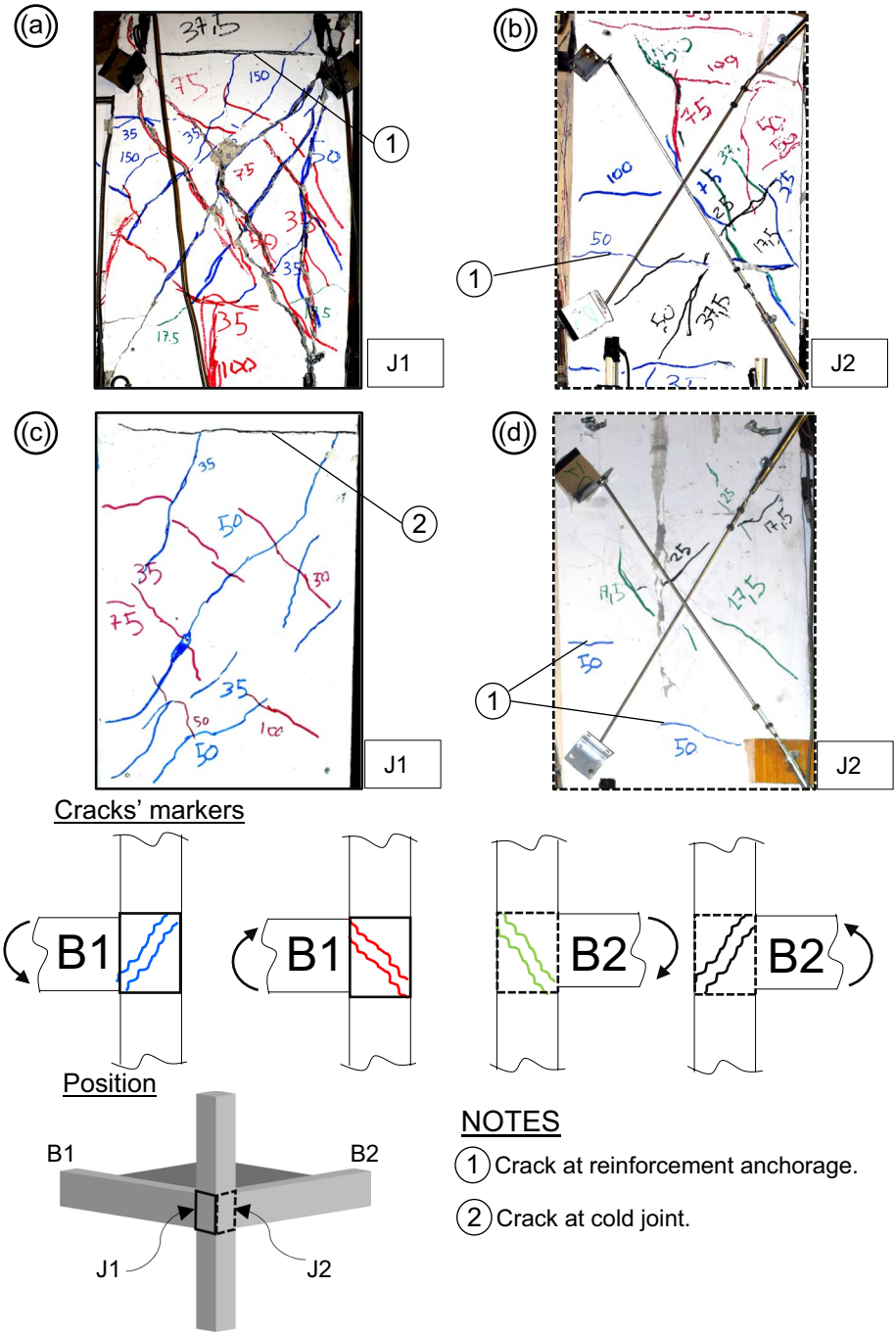

Fig. 19 Tests' results: cracks pattern at joint for (**a**–**b**) specimen CJ02 and (**c**–**d**) specimen CJ03. (Notes. The Reader is referred to the color version of this figure)

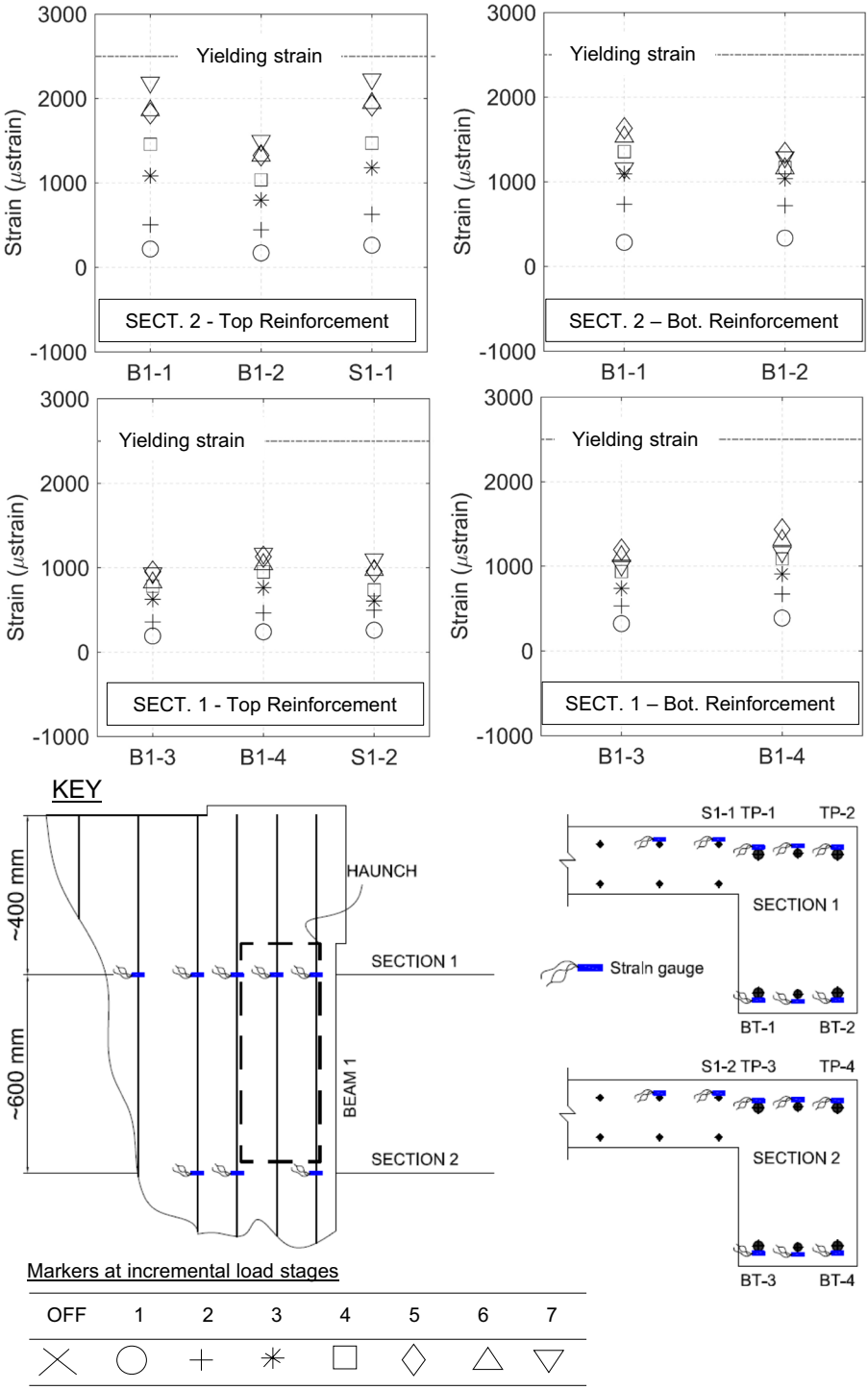

Fig. 20 Test's results: strains measured at B1 of specimen CJ03 when B2 was unloaded

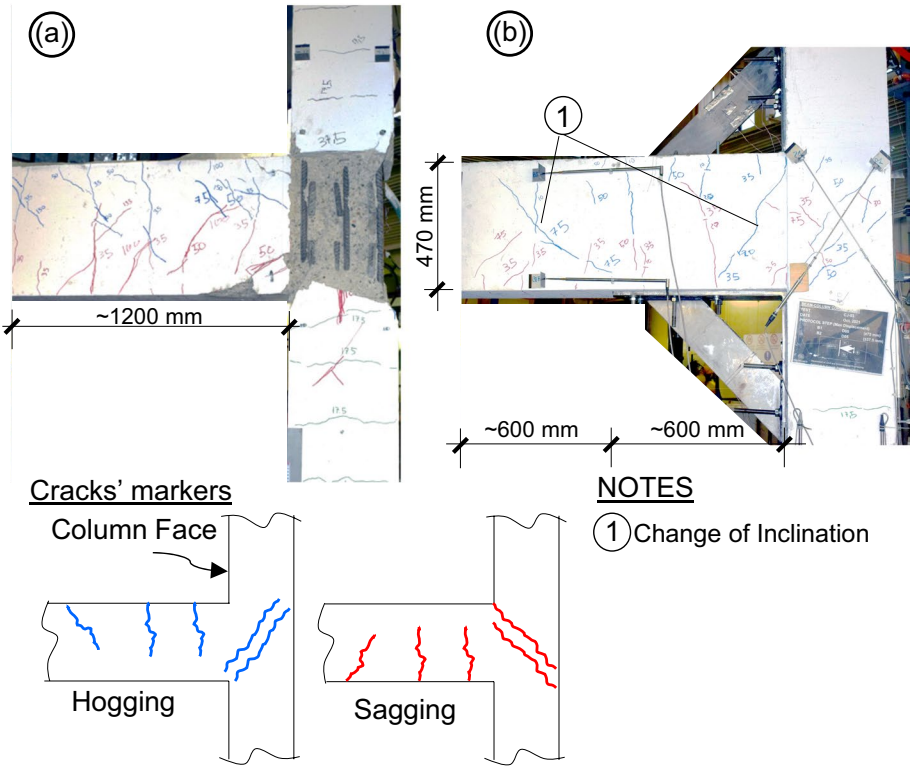

Fig. 21 Tests' results: final crack pattern at B1 for **a** specimen CJ02 and **b** specimen CJ03. (Notes. The Reader is referred to the color version of this figure)

4 Discussion

4.1 Influence of bi–axial load on joint shear strength

Joint's shear strength obtained in test CJ02 has been compared to a database of corner joints discussing the possible influence of bi–axial load protocols. The data collection was made while surveying the studies presented in Table 2. The database is given, as an appendix, in Table 8. To homogenize data, the two flexural planes of tested corner joints are termed as B1 and B2.

All the surveyed experimental campaigns assumed equal beams' cross–sections for both B1 and B2. Few specimens were characterized by non–symmetric layers of beams' reinforcement, i.e. $\rho_{s1} \neq \rho_{s2}$. Joints were unreinforced in most of the cases. During tests, column's axial load was either constantly imposed or varied proportionally to the applied shear (e.g. Akguzel and Pampanin 2010a). At peak stage, v ranged between −0.1 (tension) and 0.45 (compression).

Joint's shear failure was reported for all the tests. Not all the studies presented results for both B1 and B2. Stresses at joint (i.e. v_j, p_t and p_c) were either retrieved from

original publications or re–derived from the peak loads using Eqs. (6), (7), (8). The experimentally–derived stresses were compared to reference values such as:

- According to Priestley (1997), $p_t = 0.58\sqrt{f_c}$ and $p_c = 0.45\ f_c$;
- According to ASCE (2017), $v_j = 0.66\sqrt{f_c}$ or $0.49\sqrt{f_c}$ which are prescribed for joint with or without slab, respectively. Such distinction generally acknowledges the beneficial confinement due to transverse beam, e.g. Durrani and Zerbe (1987) and Otani (1991).

Figure 22 shows the influence of the C.F. on joint's shear strength. For moderate value of column's axial compression (e.g. $\nu < 0.25$), v_j decreases as C.F increases. As expected, the same trend can be inferred by considering p_t. Nonetheless, all these joints proved to have $p_c < 0.45f_c$ thus failure can be primarily associated to high shear stresses. Besides, experimental result obtained by Hassan (2011) ($\nu < 0$; C.F. = 1.0) may be considered as an outlier. In fact, largest reduction on both v_j and p_t should be expected for this case but experimental results do not match such intuition.

Generally, the observed trend (i.e. either v_j or p_t versus C.F.) could be explained as a consequence of confinement effect. Indeed, for C.F.<0.5 (e.g. hexagonal protocol) peaks are not simultaneous thus the largest shear demand at joint (e.g. B1) is attained when B2 is unloaded therefore the shear strength should be the one of a 2D joint augmented by confinement of a transverse beam. Conversely, for C.F.>0.5 (e.g. cloverleaf protocol), peaks are simultaneous therefore detrimental effect of bi–axial shear is dominant with respect to confinement. However, combination of bi–axial stresses is not easy–to–handle analytically

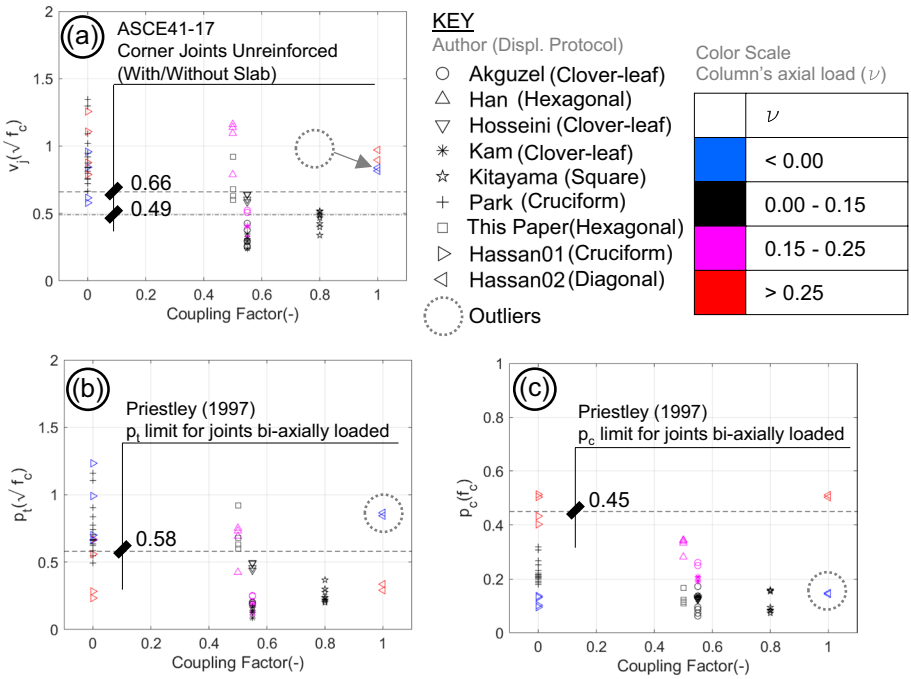

Fig. 22 Influence of Coupling Factor on joint's shear strength: **a** joint's shear stress; principal **b** tensile and **c** compressive stresses. (Notes. The Reader is referred to color version of this figure)

thus to further scrutinize the issue, a numerical investigation was carried out as discussed in the following.

Mechanical response of both uni–axially and bi–axially loaded (diagonal) joints was investigated using brick finite elements for concrete and truss elements for steel (perfectly bonded). Software (Strand7 2010) was used for numerical analyses. Modeling was generally inspired by Paulay and Priestley (1992) who, by describing two–dimensional RC beam–column joints, conveniently assumed the joint as a continuous part of the column substituting the beam with its internal forces at column–face. In this regard, a column having dimension similar to the tested specimens (350 × 350 mm cross–section, 3000 mm height) was modeled as shown in Fig. 23. Horizontal settlements (in x and y directions) of both top and bottom column's ends were imposed to simulate seismic condition. Restraints at two joint's faces were given such that the reactions amount to bending moment (and shear) which would have been transferred to beams. To the scope, compression–only springs aimed at simulating compression transfer while tensile stresses were taken by reinforcement bars which were assumed linear–elastic.

Drucker–Prager (D–P) strength criterion (reviewed by Chen 2007) was adopted for all the brick elements with the exception of the ones in the vicinity of the restraints which were linear–elastic. Elements' size were equal to 87 × 87 × 55 mm and 87 × 87 × 315 mm inside and outside the joint volume, respectively. Joint was unreinforced however stirrups (linear–elastic) were adopted outside the joint volume to prevent shear failure of the column. The percentage of column's longitudinal reinforcement (ρ_v) was equal to 1.86% as it was in specimen CJ02. Elastic–plastic material was assigned to steel being the yielding stress (f_y) equal to 530 MPa. The Authors are aware, though, that results might be impacted by an increase (or decrease) of both ρ_v and f_y. For example, Vollum and Newman (1999) acknowledged that column's vertical reinforcement (especially intermediate bars) contributes in resisting joint's shear demand.

To define the D–P's failure surface, friction angle (Φ) and cohesion (c) were assigned according to provisions given by Arslan (2007) for shear–critical beams, i.e. $\Phi = 37°$ and $c = 2.16$ MPa. The latter was obtained from empirical formula $c = 0.75f_c^{0.31}$, having assumed 30.3 MPa as concrete compressive strength (f_c). Besides, elastic modulus of concrete was taken as $4.73f_c^{0.5}$ (GPa), according to Neville (1996). Incremental displacements were

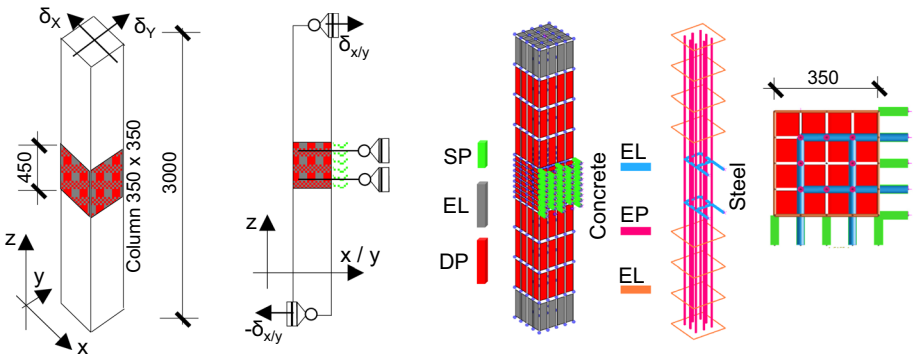

Fig. 23 Numerical model of corner joint using brick finite elements and non–linear concrete material. (Notes. Dimensions are given in millimeters. EL: Elastic material. EP: Elastic–Plastic material. DP: Drucker-Prager material. SP: Compression–only spring. The Reader is referred to the color version of this figure)

imposed up to a total drift value (sum of column's flexure and joint's distortion) equal to 2% in both x and y planes.

Three were the cases studied: (1) Uni–axial, i.e. drift was applied only x–direction; (2) Bi–axial, such that in–phase bending moments resulted at joint; (3) Bi–axial, such that out–of–phase bending moments resulted at joint. The first case was studied either with or without transversal passive confinement given by compression–only springs. No axial load was applied to the column.

Figure 24a shows the load–to–drift curves in the x–z plane (similar results were obtained in the y–z plane). All the numerical tests showed load values less than the one which corresponds to the bending failure of the column evaluated both nominally (curve labeled "Column's yielding" in the figure) and numerically (curve labeled "LE joint" in the figure). The former was obtained from sectional analysis. As for the latter, linear–elastic concrete was assigned to the joint volume whereas D–P material for the remaining parts. All the other numerical tests assumed D–P material for the joint, thus plastic development was mainly resulting from its distorsional behavior.

Figure 24b shows the numerically–derived shear stresses–to–distortion curves. Average of tangential stresses was taken at the middle–plane passing through the joint volume (see Fig. 24c). Joint's distortion was assumed as the average of the shear strains numerically–derived at Gauss points inside the joint's volume. Generally, D–P strength criterion with associative flow rule does not possess enough accuracy for deformation analysis thus the presented discussion is primarily based on strength. Numerically–derived strengths were compared to analytical predictions, i.e. Priestley (1997) and ASCE (2017). Comparison to experimentally–derived results is given as well.

Shear stress–to–distortion curves are characterized bi–linear envelope typical of D–P's material response. The shear stress obtained for 0.6% of shear distortion was taken as nominal strength. Such assumption was mainly encouraged by the envelope given by Priestley (1997) which assumes constant value of shear stress between 0 and 0.6% of shear distortion. Therefore, only in this interval the joint's response can be predicted by simple strength criterion such as D–P's one. On the contrary, larger values of shear distortion would imply abrupt increase of damage which should be investigated more properly with a refined constitutive law for concrete material, e.g. Concrete–Damage–Plasticity proposed by Lubliner et al. (1989) or Modified–Compression–Field–Theory by Vecchio and Collins (1986).

Strength's increase was noted for uni–axially loaded joint with passive confinement as a result of restrained joint's lateral expansion. Bi–axially loaded joints showed reduced shear strength if compared to the uni–axial case. The lowest shear strength was obtained for in–phase load combination. As expected, experimentally–derived strength was comparable to confined joint loaded uniaxially. In fact, although the joint has been tested bi–axially, for hexagonal load protocol (C.F.=0.5) the beneficial effect of confinement is dominant.

Figure 24c shows the joint's deformed shape and principal stresses trajectories at the end of numerical tests. After reaching the plastic surfaces, tensile stresses approached a constant value almost equal to the tensile strength of concrete. Compressive stresses were larger than nominal concrete strength due to the beneficial effect of hydrostatic stress–state which was much more promoted in bi–axial load cases when compressive trajectories concurred.

Finally, it is worth to mention that longitudinal bars of the column were activated in the resistant mechanism reaching yielding in bi–axially loaded joints.

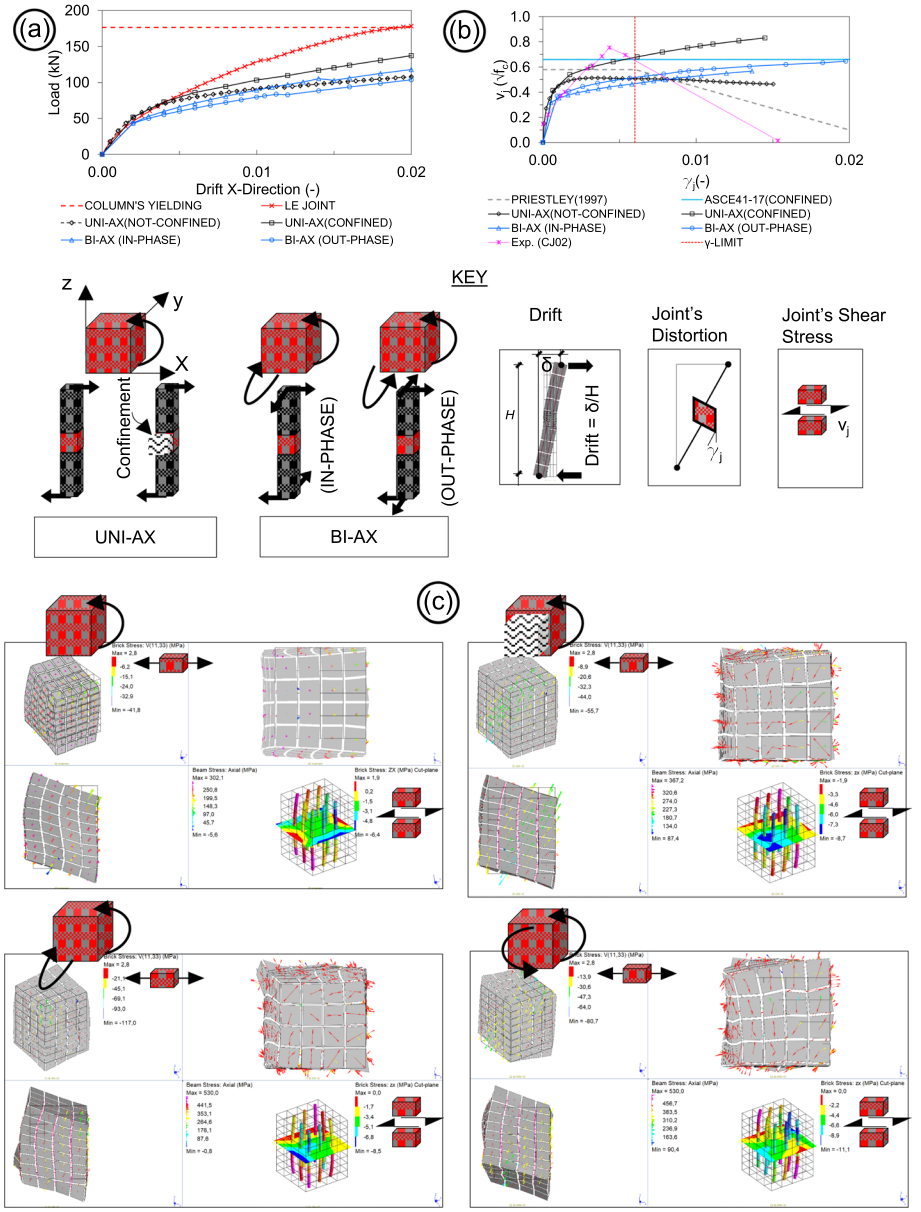

Fig. 24 Numerical results of bi–axially loaded corner joint modeled with brick finite element and concrete non–linear material: **a** load–to–drift curves; **b** shear stress–to–distortion curve; **c** stresses numerically–derived at joint. (Notes. In (c): the deformed shape was arbitrarily magnified for representation purpose; average of stresses are shown at the end of numerical test; yielding stress of reinforcement was equal to 530 MPa; concrete compressive strength was equal to 30.3 MPa. The Reader is referred to the color version of this figure)

4.2 Slab's participation in flexural behavior

To investigate slab's participation, experimentally–derived moment–curvature diagrams for beam B1 (the most loaded in hexagonal protocol), were compared to analytical predictions. For the former, curvature was derived from strains measured at reinforcement which were assumed equal to the adjacent concrete fibers due to perfect bond condition. Bending moment was obtained from free–body equilibrium of beam–column joint under the application of measured beam's shear. The envelope of the hysteretic loops was considered. Cross–section of interest were column–face and haunch's end for CJ02 and CJ03, respectively.

To derive analytical diagrams, an equivalent L–shaped cross–section was studied under flexure using the software Response–2000 (described in Sect. 3). Mean values were used for the material parameters. Different cases for slab participation were studied: (i) No slab's participation; (ii) Flange width equal to one times and (iii) Two times the slab's thickness. The latter represents the provisions given in EC8 (2004).

Comparison is given in Fig. 25. As expected, L-shaped cross–section is characterized by increased hogging moment capacity and stiffness if compared to bare rectangular cross–section. However, reduction of ductility is noted as well. Sagging behavior is almost not affected. At failure, yielding of the reinforcement was attained for all cases of slab's participation studied analytically. It can be noticed how the envelope of the experimental results, for CJ03 specimen, is comparable to analytically–derived curves. However, as mentioned in Sect. 3, full development of ductility was not possible during the experiment having reached the maximum available stroke of the hydraulic cylinders.

4.3 Application of STM

STM was employed to study the stress–field of bi-axially loaded RC corner joints tested experimentally. Figure 26a shows the equivalent truss adopted to evaluate the stress–field in discrete fashion. Structural analyses were carried out using RSTAB–8 software, developed by Dlubal (2013). Modeling was based on the following assumptions:

(i) Longitudinal reinforcement layers were lumped in four equivalent bars both for beams and column.
(ii) Struts' width was assumed equal to eight times the longitudinal bars diameters according to ACI (2021) for both beams and column. The inclination angles were generally assumed equal to 45° as can be inferred from Fig. 26c–d. Since a three–dimensional compressive field was expected within the joint volume, a first trial triangulation of struts was employed as shown in Fig. 26b. Afterward, equilibrated condition was searched iteratively being the struts able to carry only compression forces.
(iii) Nodes of the equivalent truss were considered smeared according to Schlaich et al. (1987). Local crushing of concrete has been not considered.
(iv) Slab was modeled as a membrane by using a plane grid of reinforcement and triangulation of compression–only struts. For the latter, since the direction of compression cannot be easily established a priori, similar trial-and-error procedure was employed as the one adopted for the joint's struts. For the sake of validation, the envelope of activated struts for the leading load cases (peak hogging for B1 and simultaneous peak hogging for B1 and B2) was compared to the observed crack pattern at slab's extrados. Results are shown in Fig. 27.

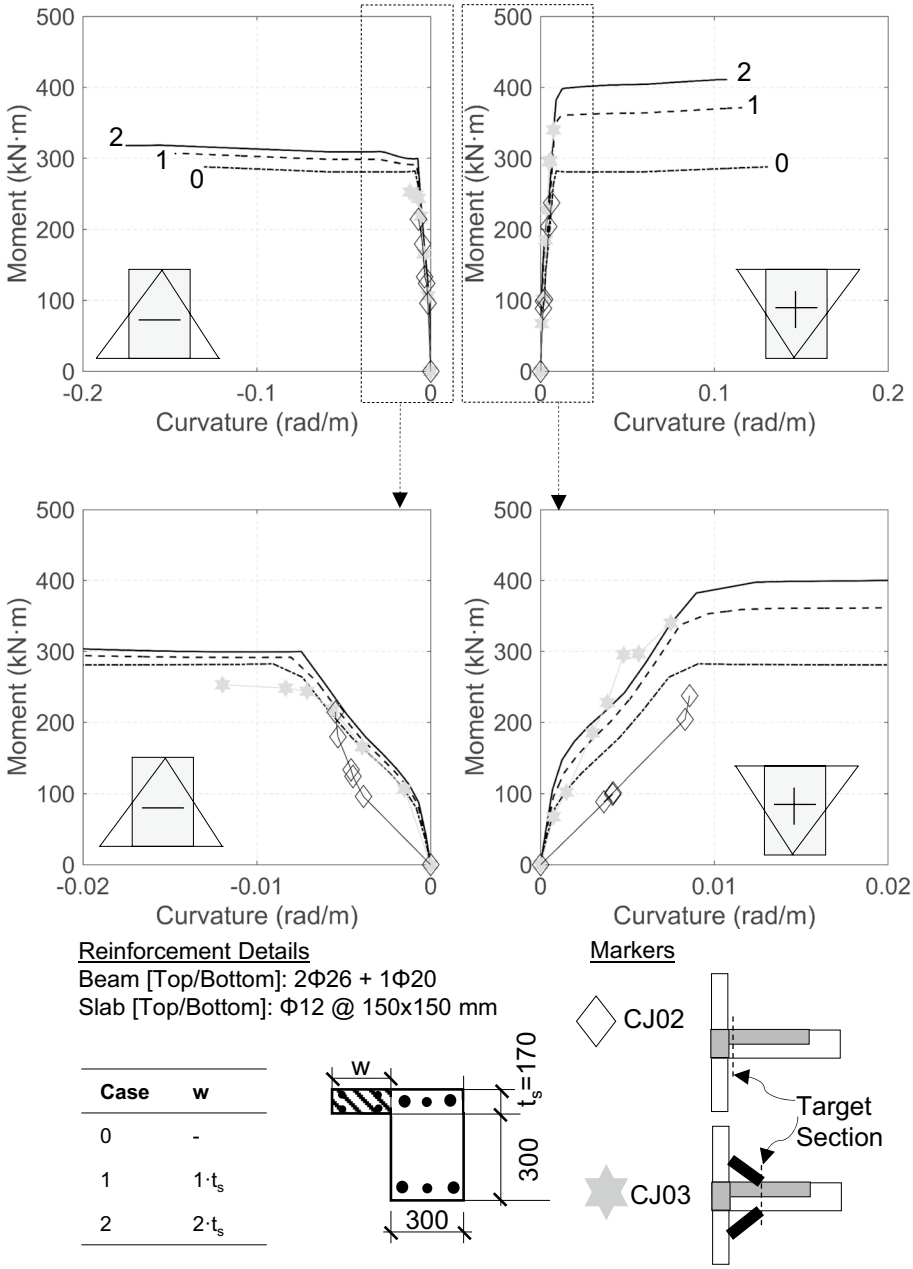

Fig. 25 Comparison between analytically–derived and experimentally–derived moments and curvatures for different slab's participation

(v) Additional compressive struts were used to explore the torsional behavior of beams.

Axial forces predicted using STM model were compared to experimentally–derived ones, which were obtained from load conversion of measured strains. In this regard, it

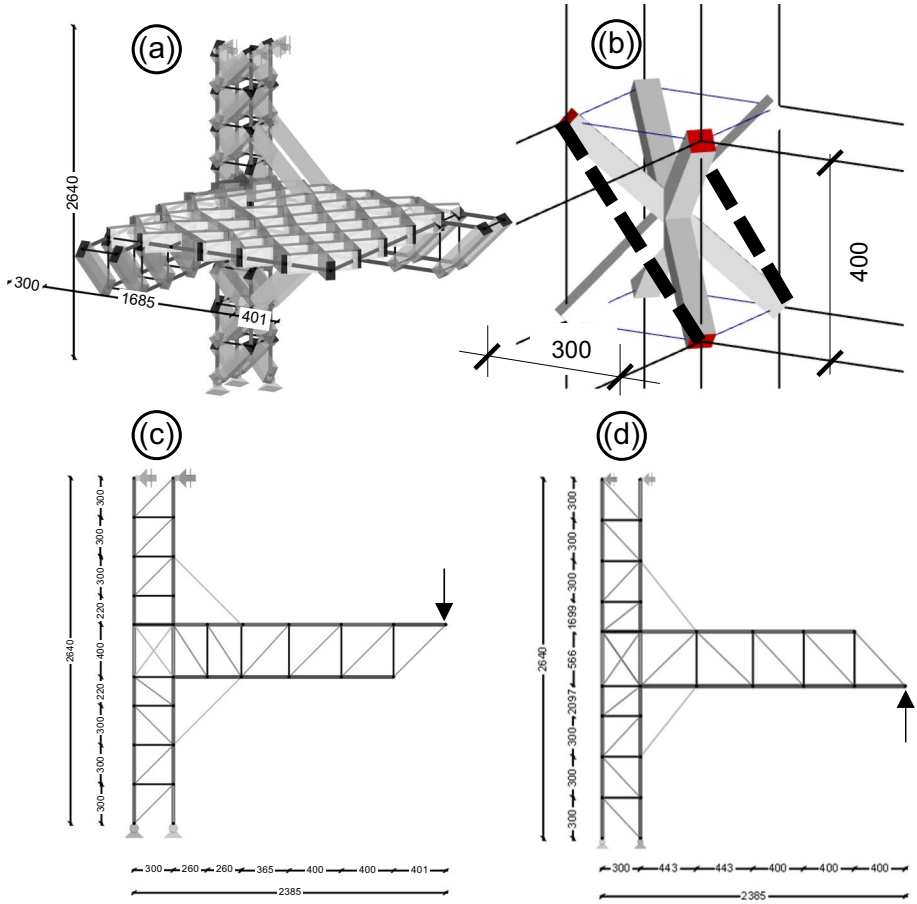

Fig. 26 STM application to corner joint retrofitted with haunch: **a** three–dimensional equivalent truss; **b** detail of investigated compression trajectories inside the joint's volume; **c** two–dimensional view of the equivalent truss used for hogging behavior; **d** two–dimensional view of the equivalent truss used for sagging behavior. (Notes. Dimensions are given in millimeters)

was verified that linear–elastic behavior of steel was maintained during the tests. For example, Fig. 28 shows the peaking of strains both for haunch diagonal and reinforcement for specimen CJ03. For the selected load stages, only B1 was loaded whereas B2 was unloaded. Strains proved to be below the nominal yielding threshold. Since haunch diagonal's strains were not constant across the width, an average value was assumed when deriving the axial force. As per STM, axial forces were obtained by applying concentrated loads, at beams' ends, equal to the experimentally–measured ones.

Two are the axial forces crucial in haunch retrofit design, namely (i) Axial force of the beam's longitudinal reinforcement at column–face (F_L) and (ii) Haunch's diagonal force (F_H). The former, according to Eq. (6), is linearly dependent to the shear demand at joint. The latter is decisive in sizing the haunch element and its connection to concrete.

Compared axial forces, at peak stages, are reported in Table 7. For the sake of completeness, forces obtained using β–factor approach (introduced in Sect. 3.4) are reported as well. STM proved to predict conservatively both F_L and F_H. Differences recognized for β–factor

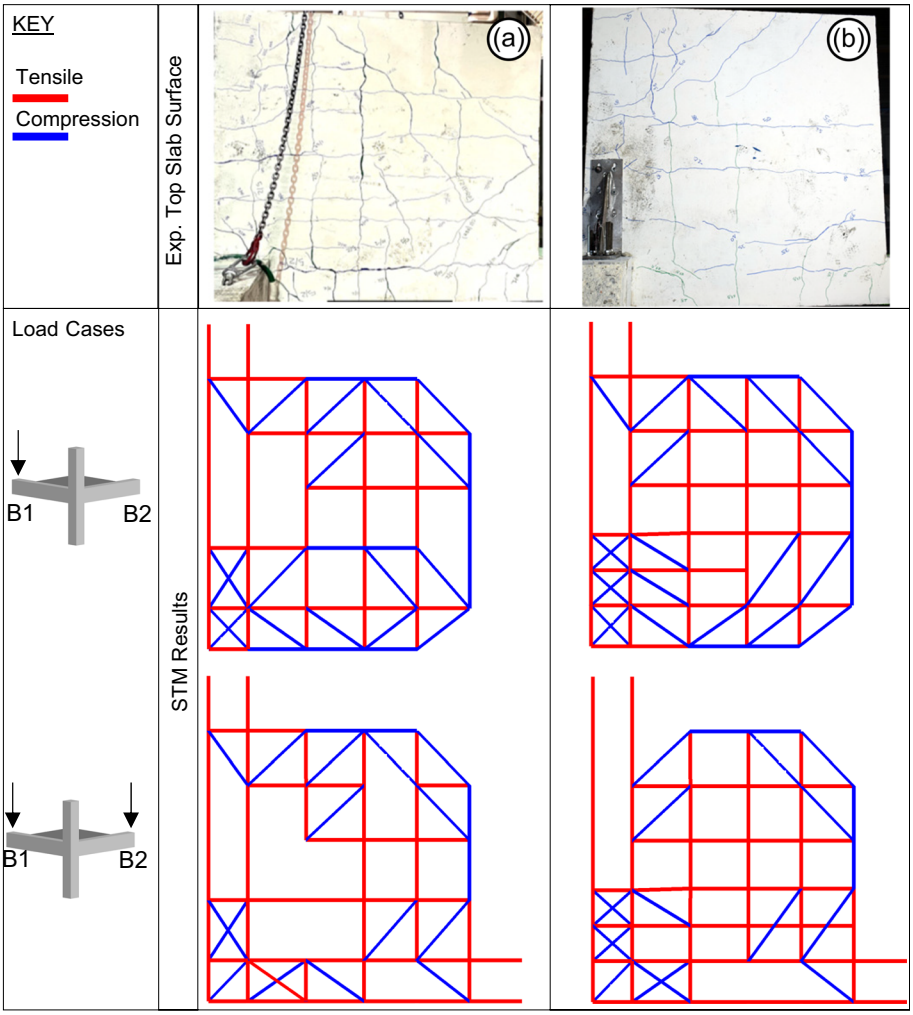

Fig. 27 Comparison between the experimental crack pattern at slab's estrados and STM compressive struts obtained for leading load cases: **a** specimen CJ02; **b** specimen CJ03. (Notes. The Reader is referred to the color version of this figure)

approach might be ascribed to inconsistent compatibility conditions which, according to Marchisella and Muciaccia (2023), mainly characterize extended haunches as the one adopted in the presented experimental campaign.

5 Conclusion

This paper focused on RC beam–column joints bi–axially loaded and application of haunch retrofit. Three were the investigations scopes and the following conclusions are given in their regard.

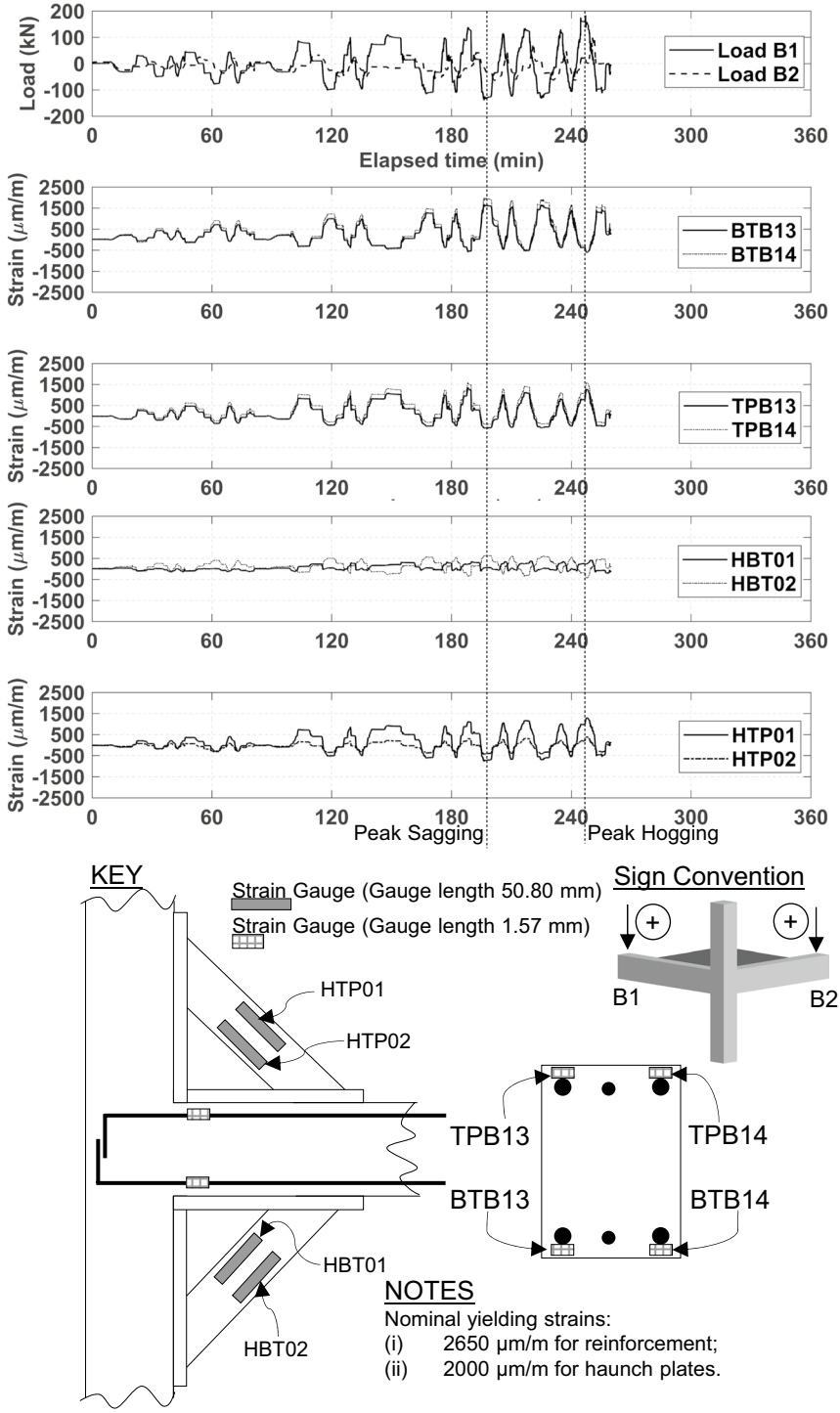

Fig. 28 Peaking of experimentally–measured strains, for specimen CJ03

Table 7 Comparison between experimentally–derived internal forces, STM and β-factor approach

TEST	Dir.[a]	$V_b^{(b)}$ (kN)	$F_L^{(c)}$ (kN) / (T−t−P)					$F_H^{(d)}$ (kN) / (T−t−P)				
		Exp	Exp	STM		β		Exp	STM		β	
CJ02	(+)	102	545	524	1.04	–	–	–	–	–	–	–
	(−)	114	719	594	1.21	–	–	–	–	–	–	–
CJ03	(+)	148	372	343	1.08	200	1.85	124	185	0.67	137	0.90
	(−)	125	413	401	1.03	173	2.38	158	178	0.88	115	1.37

(a) Load direction: (+) hogging–type moment, for the beam, at column–face; (−) sagging–type moment, for the beam, at column–face

(b) Beam's shear at peak

(c) Axial force of the beam's longitudinal reinforcement. Experimentally–derived values were obtained from load conversion of strains

(d) Axial force of the haunch's diagonal. Experimentally–derived values were obtained from load conversion of strains

First, mechanical response of a corner joint under bi–axial shear is different from that of an identical joints uniaxially loaded. Bi–axial load protocol, defined by the Coupling Factor (C.F.), can influence the strength for moderate values of column's axial compression (ν), e.g. ν <0.25. By considering a database of corner joints tested bi–axially, for C.F.<0.5 (i.e. non–simultaneous peaks) joint's shear strength was higher than analytically–derived prediction. For C.F.>0.5 (i.e. simultaneous peaks), strength's reduction was evident. Such result was explained as combination of both beneficial effect of joint's confinement, which prevails in the first case, and (ii) detrimental effect of bi–axial shear demand. In many design circumstances (RC buildings characterized by regularity in plan) it might be not practical to evaluate shear demand orbitals at joint and their associated C.F. In such cases C.F.<0.5 is generally expected therefore it is recommended to use nominal strength's provisions for bi–axially loaded joints which are given either by design guidelines or by literature. High level of structural analysis approximation should be adopted for non–regular buildings.

Second, haunch retrofit was employed to promote beam's hinging of a shear critical corner joint. Hexagonal bi–axial load protocol was used because it has two major advantages: on one hand is comparable to the elliptical envelope which most probably represents bi–axial shear demand at corner joints for regular buildings (a brief case study was presented); on the other is easy to implement experimentally. Experimental results showed a significant reduction of both joint's distortion and shear stress for the retrofitted joint. Inversion of the shear cracks inclination was recognized at the column–face. Slab's participation and torsional behavior were confirmed both by the observed crack pattern and strains at reinforcement.

Third, internal forces of haunch retrofitted joint were analytically–derived from an application of Strut-and-Tie model (STM) which adopts equivalent truss. In particular, three-dimensional grid of struts is needed to model compressive field of both slab's membrane response and beam's torsion. By comparing both the haunch force and the joint's shear demand to experimentally–derived values, agreement was found.

Appendix 1: Database of beam–column joints (corner type)

This appendix contains database of beam–column joints (corner type). Data were collected from technical literature published in English (Table 8).

Table 8 Database of RC corner joints tested bi–axially

Test	S (a) (−)	w/t (b) (−)	ρ_{s1} (c) (%)	ρ_{s2} (d) (%)	ρ_h (e) (%)	ν (f) (−)	B (g) (−)	D (h) (±)	v_j (i) ($\sqrt{f_c}$)	p_t (j) ($\sqrt{f_c}$)	p_c (k) (f_c)	F. (j) (−)
Akguzel and Pampanin (2010b)												
3DB1	×	–	0.5	0.5	0.1	0.04	1	(+)	0.26	0.19	0.07	JS
3DB2	×	–	0.5	0.5	0.0	0.11	1	(+)	0.43	0.25	0.17	JS
3DB1	×	–	0.5	0.5	0.1	0.02	2	(+)	0.25	0.20	0.06	JS
3DB2	×	–	0.5	0.5	0.0	0.08	2	(+)	0.38	0.25	0.14	JS
3DB1	×	–	0.5	0.5	0.1	0.06	1	(−)	0.30	0.19	0.10	JS
3DB2	×	–	0.5	0.5	0.0	0.20	1	(−)	0.52	0.25	0.26	JS
3DB1	×		0.5	0.5	0.1	0.05	2	(−)	0.29	0.20	0.09	JS
3DB2	×	–	0.5	0.5	0.0	0.19	2	(−)	0.51	0.25	0.25	JS
Han and Lee (2020)												
JOB	✓	15	0.5	0.5	0.2	0.20	1	(−)	0.43	0.75	0.34	JS
JOB	✓	15	0.5	0.5	0.2	0.20	1	(+)	0.58	0.73	0.34	JS
Hosseini et al. (2018)												
CRC	×	–	0.7	0.7	0.5	0.05	1	(+)	0.59	0.44	0.12	JS
CRC	×	–	0.7	0.7	0.5	0.05	1	(+)	0.64	0.49	0.13	JS
CRC	×	–	0.7	0.7	0.5	0.05	2	(−)	0.60	0.46	0.13	JS
CRC	×	–	0.7	0.7	0.5	0.05	2	(−)	0.64	0.50	0.13	JS
Kam et al. (2010)												
3DB	×	–	0.4	0.4	0.0	0.16	1	(−)	0.33	0.13	0.20	JS
3DB	×	–	0.4	0.4	0.0	0.16	1	(+)	0.41	0.19	0.21	JS
3DB	×	–	0.4	0.4	0.0	0.16	2	(−)	0.29	0.11	0.19	JS
3DB	×	–	0.4	0.4	0.0	0.16	2	(+)	0.40	0.18	0.21	JS
3DS	✓	11	0.4	0.4	0.0	0.11	1	(−)	0.30	0.13	0.13	JS
3DS	✓	11	0.4	0.4	0.0	0.11	1	(+)	0.35	0.17	0.14	JS
3DS	✓	11	0.4	0.4	0.0	0.11	2	(−)	0.24	0.09	0.13	JS
3DS	✓	11	0.4	0.4	0.0	0.11	2	(+)	0.31	0.14	0.14	JS
Kitayama and Katae (2017)												
K2	×	–	1.1	1.1	0.3	0.04	1	(−)	0.50	0.37	0.09	JS
K2	×	–	1.1	1.1	0.3	0.04	1	(−)	0.40	0.28	0.08	JS
K3	×	–	1.1	1.1	0.3	0.13	1	(−)	0.52	0.24	0.16	JS
K3	×	–	1.1	1.1	0.3	0.13	1	(−)	0.48	0.21	0.16	JS
K2	×	–	1.1	1.1	0.3	0.04	2	(−)	0.34	0.22	0.07	JS
K2	×	–	1.1	1.1	0.3	0.04	2	(−)	0.42	0.30	0.08	JS
K3	×	–	1.1	1.1	0.3	0.13	2	(−)	0.47	0.20	0.15	JS
K3	×	–	1.1	1.1	0.3	0.13	2	(−)	0.51	0.24	0.16	JS
Marchisella (2022)												
CJ02	✓	8	0.8	0.8	0.0	0.00	1	(+)	0.68	0.68	0.12	JS
CJ02	✓	8	0.8	0.8	0.0	0.00	1	(−)	0.92	0.92	0.17	JS
CJ02	✓	8	0.8	0.8	0.0	0.00	2	(+)	0.60	0.60	0.11	JS
CJ02	✓	8	0.8	0.8	0.0	0.00	2	(−)	0.63	0.63	0.11	JS
Hassan (2011)												
UJ1	✓	11	1.8	1.4	0.0	0.31	1	(+)	1.26	0.67	0.43	JS

Table 8 (continued)

Test	S (a) (−)	w/t (b) (−)	ρ_{s1} (c) (%)	ρ_{s2} (d) (%)	ρ_h (e) (%)	ν (f) (−)	B (g) (−)	D (h) (±)	v_j (i) ($\sqrt{f_c}$)	p_t (j) ($\sqrt{f_c}$)	p_c (k) (f_c)	F. (j) (−)
UJ1	✓	11	1.8	1.4	0.0	−0.09	1	(−)	0.96	1.23	0.14	JS
UJ1	✓	11	1.8	1.4	0.0	0.30	2	(+)	1.11	0.56	0.40	JS
UJ1	✓	11	1.8	1.4	0.0	−0.05	2	(−)	0.84	0.99	0.13	JS
UJ2	✓	11	0.8	0.7	0.0	0.46	1	(+)	0.88	0.28	0.51	JS
UJ2	✓	11	0.8	0.7	0.0	−0.03	1	(−)	0.62	0.70	0.10	JS
UJ2	✓	11	0.8	0.7	0.0	0.46	2	(+)	0.79	0.23	0.50	JS
UJ2	✓	11	0.1	0.1	0.0	−0.03	2	(−)	0.58	0.66	0.10	JS
BJ1	✓	11	1.8	1.4	0.0	0.45	1	(+)	1.03	0.34	0.51	JS
BJ1	✓	11	1.8	1.4	0.0	−0.01	1	(−)	0.89	0.87	0.15	JS
BJ1	✓	11	1.8	1.4	0.0	0.45	2	(+)	0.95	0.29	0.50	JS
BJ1	✓	11	1.8	1.4	0.0	−0.01	2	(−)	0.86	0.84	0.14	JS
Park and Mosalam (2013)												
SP1	✓	13	0.6	0.6	0.0	0.08	1	(+)	0.84	0.66	0.22	JS
SP2	✓	13	1.1	0.8	0.0	0.08	1	(+)	1.30	1.11	0.31	JS
SP3	✓	13	0.4	0.4	0.0	0.08	1	(+)	0.81	0.64	0.21	JS
SP4	✓	13	0.7	0.5	0.0	0.07	1	(+)	0.95	0.77	0.22	JS
SP1	✓	13	0.6	0.6	0.0	0.08	1	(−)	0.92	0.74	0.23	JS
SP2	✓	13	1.1	0.8	0.0	0.08	1	(−)	1.09	0.91	0.27	JS
SP3	✓	13	0.4	0.4	0.0	0.08	1	(−)	0.76	0.58	0.20	JS
SP4	✓	13	0.7	0.5	0.0	0.07	1	(−)	0.88	0.70	0.21	JS
SP1	✓	13	0.6	0.6	0.0	0.08	2	(+)	0.80	0.62	0.21	JS
SP2	✓	13	1.1	0.8	0.0	0.08	2	(+)	1.35	1.16	0.32	JS
SP3	✓	13	0.4	0.4	0.0	0.08	2	(+)	0.72	0.55	0.19	JS
SP4	✓	13	0.7	0.5	0.0	0.07	2	(+)	0.84	0.67	0.20	JS
SP1	✓	13	0.6	0.6	0.0	0.08	2	(−)	0.85	0.67	0.22	JS
SP2	✓	13	1.1	0.8	0.0	0.08	2	(−)	1.02	0.84	0.25	JS
SP3	✓	13	0.4	0.4	0.0	0.08	2	(−)	0.66	0.49	0.18	JS
SP4	✓	13	0.7	0.5	0.0	0.07	2	(−)	0.75	0.58	0.19	JS

(a) Specimen with slab

(b) Width-to-thickness ratio of the slab

(c)-(d) Beam's longitudinal reinforcement ratio in direction 1 and 2, respectively

(e) Hoops ratio

(f) Normalized column's axial force at peak stage, i.e. $\frac{N}{A_c \cdot f_c}$

(g) Considered beam's, i.e. Beam 1 or Beam 2

(h) Considered load direction, viz. positive is providing hogging bending moment at column–face

(i) Joint's shear stress according to Eq. (6)

(j) Principal tensile stress according to Eq. (7)

(k) Principal compressive stress according to Eq. (8)

(l) Failure mode: (JS) indicates joint's shear failure

Acknowledgements The authors wish to express their gratitude to the Material Testing Laboratory of Politecnico di Milano for supporting the experimental campaigns. Special thanks should be conveyed to Daniele Spinelli, Andrea Consiglio, Giuseppe Di Nunzio, for their assistance in implementing the test setup. Finally, Prof. Gianpaolo Rosati is acknowledged for his guidance during the experimental campaign.

Author contributions Conceptualization: AM/GM; Methodology: AM/GM; Data analysis: AM; Software: AM; Visualization: AM; Writing–Original Draft: AM; Writing–Reviews: AM/GM.

Funding Open access funding provided by Politecnico di Milano within the CRUI-CARE Agreement. The authors have not received any funding.

Data availability Data are available upon request.

Declarations

Conflict of interest The Authors declare no conflict of interest.

Consent to participate Both the Authors intended to submit this paper to BEEE.

Consent for publication Both the Authors intended to publish this paper in BEEE.

Open Access This article is licensed under a Creative Commons Attribution 4.0 International License, which permits use, sharing, adaptation, distribution and reproduction in any medium or format, as long as you give appropriate credit to the original author(s) and the source, provide a link to the Creative Commons licence, and indicate if changes were made. The images or other third party material in this article are included in the article's Creative Commons licence, unless indicated otherwise in a credit line to the material. If material is not included in the article's Creative Commons licence and your intended use is not permitted by statutory regulation or exceeds the permitted use, you will need to obtain permission directly from the copyright holder. To view a copy of this licence, visit http://creativecommons.org/licenses/by/4.0/.

References

ACI (2002) 352R-02 Recommendations for design of beam-column connections in monolithic reinforced concrete structures (ACI-ASCE 352-02). American Concrete Institute

ACI (2015) 374.2R-13 Guide for testing reinforced concrete structural elements under slowly applied simulated seismic loads, vol 3. American Concrete Institute

ACI (2019) 318-19 Building code requirements for structural concrete and commentary. American Concrete Institute, https://doi.org/10.14359/51716937

ACI (2021) PRC-445.2-21: Strut-and-Tie Method Guidelines for ACI 318-19

Akguzel U, Pampanin S (2010) Effects of variation of axial load and bidirectional loading on seismic performance of GFRP retrofitted reinforced concrete exterior beam-column joints. J Compos Constr 14(1):94–104. https://doi.org/10.1061/(ASCE)1090-0268(2010)14:1(94)

Akguzel U, Pampanin S (2010) Effects of variation of axial load and bidirectional loading on seismic performance of GFRP retrofitted reinforced concrete exterior beam-column joints. J Compos Constr 14(1):94–104. https://doi.org/10.1061/(ASCE)1090-0268(2010)14:1(94)

Alaee P, Li B, Cheung PP (2015) Parametric investigation of 3D RC beam-column joint mechanics. Mag Concr Res 67(19):1054–1069. https://doi.org/10.1680/macr.15.00005

Antoniou S (2023) Seismic retrofit of existing RC buildings. Wiley-Blackwell, New Jersey. https://doi.org/10.1002/9781119987352

Arslan G (2007) Sensitivity study of the Drucker–Prager modeling parameters in the prediction of the nonlinear response of reinforced concrete structures. Mater Des 28(10):2596–2603. https://doi.org/10.1016/j.matdes.2006.10.021

ASCE (2017) ASCE/SEI, 41-17 Seismic evaluation and retrofit of existing buildings. June

Bentz EC (2000) Sectional analysis of reinforced concrete members. University of Toronto, Toronto

Birely AC, Lowes LN, Dawn EL (2012) Linear analysis of concrete frames considering joint flexibility. ACI Struct J 109(3):381–391. https://doi.org/10.14359/51683752

Bonacci J, Pantazopoulou S (1993) Parametric investigation of joint mechanics. ACI Struct J 90(1):61–71. https://doi.org/10.14359/4211

Burguieres J, Longwell J, Jirsa JO (1980) Shear and Bond deterioration in beam-to-column joints under bidirectional load reversals. University of Texas at Austin, Austin

Chen TH (2006) Retrofit strategy of non-seismically designed frame systems based on a metallic haunch system. University of Canterbury, Canterbury

Chen WF (2007) Plasticity in Reinforced Concrete. J. Ross Publishing, USA

Dilsiz A, Günay S, Mosalam KM, Miranda E, Arteta C, Sezen H, Fischer E, Hakhamaneshi M, Hassan WM, Alhawamdeh B, Andrus S (2023) StEER-EERI: 2023 Mw 7.8 Kahramanmaras, Türkiye Earthquake Sequence Joint Preliminary Virtual Reconnaissance Report (PVRR)

Dlubal (2013) RSTAB 8. Structural analysis of general frameworks

Durrani A, Zerbe H (1987) Seismic resistance of RC exterior connections with floor slab. J Struct Eng 113(8):1850–1864. https://doi.org/10.1061/(ASCE)0733-9445(1987)113:8(1850)

EC2 (2004) EN 1992-1-1(2014) Eurocode2: Design of concrete structures; Part 1-1: General rules and rules for buildings

EC8 (2004) EN 1998-1:2004 Eurocode 8: Design of Structures for earthquake resistance. Part1: General rules, seismic actions and rules for buildings

Elwood KJ (2010) Effective stiffness of reinforced concrete columns. ACI Struct J 107(3):372–373. https://doi.org/10.14359/56613

Engindeniz M (2008a) Performance of an RC corner beam-column joint severely damaged under bidirectional loading and rehabilitated with FRP composites. ACI Special Publication pp 25. https://doi.org/10.14359/20249

Engindeniz M (2008b) Repair and strengthening of Pre-1970 reinforced concrete corner beam-column joints using CFRP composites. PhD thesis, Georgia Institute of Technology, http://hdl.handle.net/1853/24808

Engindeniz M, Kahn LF, Zureick AH (2005) Repair and strengthening of reinforced concrete beam-column joints: state of the art. ACI Struct J 102(2):187–197. https://doi.org/10.14359/14269

Fardis MN (2009) Seismic design, assessment and retrofitting of concrete buildings. Springer, London. https://doi.org/10.1007/978-1-4020-9842-0

Fib (2022) FIB model code 2020 (2ndDraft). Part VI

Han SW, Lee CS (2020) Cyclic behavior of RC OMF beam-corner column joints under unidirectional and bidirectional loadings. Eng Struct 224(Sept.):111304. https://doi.org/10.1016/j.engstruct.2020.111304

Han SW, Lee SH (2022) Cyclic behavior of high-performance fiber-reinforced cementitious composite corner joints. J Build Eng 47(July 2021):103892. https://doi.org/10.1016/j.jobe.2021.103892

Hassan WM (2011) Analytical and experimental assessment of seismic vulnerability of beam-column joints without transverse reinforcement in concrete buildings. Phd thesis, Berkeley, https://escholarship.org/uc/item/1k49h3mx

Hassan WM, Moehle JP (2012) Experimental assessment of seismic vulnerability of corner beam-column joints in older concrete buildings. In: 15th world conference on earthquake engineering, Lisbon Portugal

Hosseini F, Gencturk B, Aryan H et al (2018) Seismic behavior of 3-D ECC beam-column connections subjected to bidirectional bending and torsion. Eng Struct 172(November 2017):751–763. https://doi.org/10.1016/j.engstruct.2018.06.054

Ishizuka H, Kitayama K (2016) Seismic performance and ultimate flexural capacity evaluation based on 3D joint-hinging failure model for R/c corner coulumn-beam joint under bi-lateral loading (Japanese). J Struct Constr Eng 81(729):1881–1891. https://doi.org/10.3130/aijs.81.1881

Kam WY, Quintana-Gallo P, Akguzel U, et al (2010) Influence of slab on the seismic response of substandard detailed exterior reinforced concrete beam column joints. In: 9th US National and 10th Canadian conference on earthquake engineering 2010, Including Papers from the 4th International Tsunami Symposium 3(January):2188–2198

Kitayama K, Katae H (2017) Earthquake resistance of reinforced concrete corner beam-column joints with different column axial loads under bidirectional lateral loading. Bull N Z Soc Earthq Eng 50(4):527–536. https://doi.org/10.5459/bnzsee.50.4.527-536

Kurose Y, Guimaraes G, Zuhua L et al (1991) Evaluation of slab-beam-column connections subjected to bidirectional loading. ACI Special Publ 123:39–67. https://doi.org/10.14359/2807

Leon R, Jirsa JO (1986) Bidirectional loading of RC beam-column joints. Earthq Spectra 2(3):537–564. https://doi.org/10.1193/1.1585397

Li Z, Cui Y, Song K et al (2019) The shearing performance of a beam-column joint in a reinforced concrete frame subjected to bidirectional loading. Adv Struct Eng 22(15):3176–3189. https://doi.org/10.1177/1369433219859475

Lubliner J, Oliver J, Oller S et al (1989) A plastic-damage model for concrete. Int J Solids Struct 25(3):299–326. https://doi.org/10.1016/0020-7683(89)90050-4

Mahadik V, Sharma A (2021) Bi-directional loading history for seismic testing of 3D frame joints. Civil Eng 2(2):349–369. https://doi.org/10.3390/civileng2020019

Marchisella A (2022) Seismic assessment of existing 3D RC beam-column joints and retrofit with fully fastened haunch. Politecnico di Milano, Milano

Marchisella A, Muciaccia G (2022) Comparative assessment of shear demand for RC beam-column joints under earthquake loading. Appl Sci 12(14):7153. https://doi.org/10.3390/app12147153

Marchisella A, Muciaccia G (2023) Haunch retrofit of RC beam—column joints : linear stress field analysis and Strut-and-Tie method application. Earthquake Eng Struct Dynam 52(12):3575–3599. https://doi.org/10.1002/eqe.3921

Marchisella A, Muciaccia G, Sharma A et al (2021) Experimental investigation of 3d RC exterior joint retrofitted with FFHR. Eng Struct 239(July):112206. https://doi.org/10.1016/j.engstruct.2021.112206

Menun C (2000) Envelopes for seismic response vectors. I: theory. J Struct Eng 126:467–473. https://doi.org/10.1061/(ASCE)0733-9445(2000)126:4(467)

Menun C (2000) Envelopes for seismic response vectors. II: applications. J Struct Eng 126(4):474–481. https://doi.org/10.1061/(ASCE)0733-9445(2000)126:4(474)

Miranda E (1999) Approximate seismic lateral deformation demands in multistory buildings. J Struct Eng 125(April):417–425. https://doi.org/10.1061/(ASCE)0733-9445(1999)125:4(417)

Mitchell D, Cook W, Uribe CM, et al (2002) Experimental verification of strut-and-tie models. In: ACI SP-208 examples for the design of structural concrete with Strut-and-Tie models, vol SP-208. American Concrete Institute, chap 3, pp 41–62

Negro P, Mola E, Molina FJ, et al (2004) Full-scale PsD testing of a torsionally unbalanced three-storey non-seismic RC frame. In: 13th world conference on earthquake engineering, Vancouver, 968

Neville AM (1996) Properties of concrete, 4th edn. Prentice Hall, Harlow. https://doi.org/10.1016/0008-8846(96)82366-0

Newmark NM (1975) Seismic design criteria for structures and facilities Trans-Alaska pipeline system. In: U.S. National Conference on Earthquake Engineering, pp 94–103

Nishimura K, Muraoka S, Yagiura T et al (2014) An experimental study on stress transfer in a reinforced concrete corner beam-column joint yielded in flexure at beam ends (Japanese). J Struct Constr Eng 79(699):621–630. https://doi.org/10.3130/aijs.79.621

NZSEE (2017) The seismic assessement of existing building. Tech. rep., New Zeland Society of Earthquake Engineering, http://www.eq-assess.org.nz/isa/

Opabola E, Elwood KJ, Pujol S (2020) Influence of biaxial lateral loading on seismic response of reinforced concrete columns. ACI Struct J 117(6):211–224. https://doi.org/10.14359/51728069

Ong CB, Chin CL, Ma CK, Tan JY, Awang AZ, Omar W (2022) Seismic retrofit of reinforced concrete beam-column joints using various confinement techniques: A review. Structures 42:221–243. //doi.org/10.1016/j.istruc.2022.05.114

Otani S (1991) The architectural institute of Japan proposal of ultimate strength design requirements for RC buildings with emphasis on beam-column joints. ACI Symp Publ 123:125–144. https://doi.org/10.14359/2829

Pampanin S, Christopoulos C, Chen TH (2006) Development and validation of a metallic haunch seismic retrofit solution for existing under-designed RC frame buildings. Earthq Eng Struct Dynam 44(September):657–675. https://doi.org/10.1002/eqe. arXiv:1403.5481v1

Pampanin S, Bolognini D, Pavese A (2007) Performance-based seismic retrofit strategy for existing reinforced concrete frame systems using fiber-reinforced polymer composites. J Compos Constr 11(2):211–226. https://doi.org/10.1061/(asce)1090-0268(2007)11:2(211)

Park S (2010) Experimental and analytical studies on reinforced concrete buildings with seismically vulnerable beam-column joints. University of California, Berkeley

Park S, Mosalam KM (2013) Experimental investigation of nonductile RC corner beam-column joints with floor slabs. J Struct Eng 139(1):1–14. https://doi.org/10.1061/(ASCE)ST.1943-541X.0000591

Paulay T, Priestley N (1992) Seismic design for concrete and masonry buildings. Wiley, New York

Popovics S (1973) A numerical approach to the complete stress-strain curve of concrete. Cem Concr Res 3:583–599. https://doi.org/10.1016/0008-8846(73)90096-3

Priestley N (1997) Displacement-based seismic assessment of reinforced concrete buildings. J Earthq Eng 1(1):157–192. https://doi.org/10.1080/13632469708962365

Priestley N, Calvi GM, Kowalsky M (2007) Displacement-based seismic design of structures. IUSS Press, Pavia

Quintana-Gallo P, Akguzel U, Carr AJ et al (2021) Seismic response of a non-ductile RC frame building subjected to shake-table excitations. Bull Earthq Eng 20(1):1–29. https://doi.org/10.1007/s10518-021-01228-4

Rodrigues H, Varum H, Arêde A et al (2013) Behaviour of reinforced concrete column under biaxial cyclic loading-state of the art. Int J Adv Struct Eng 5(1):1–12. https://doi.org/10.1186/2008-6695-5-4

Salami MR, Afsar Dizaj E, Kashani MM (2021) Fragility analysis of rectangular and circular reinforced concrete columns under bidirectional multiple excitations. Eng Struct 233:111887. https://doi.org/10.1016/j.engstruct.2021.111887

Sano Y, Fujima A, Ishikawa T et al (2022) Joint hinging failure of RC corner column-beam joint under varying axial and bi-lateral loads (Japanese). J Struct Constr Eng 87(792):217–228. https://doi.org/10.3130/aijs.87.217

Schlaich J, Schafer K, Jennewein M (1987) Toward a consistent design of structural concrete. PCI J 32(May):74–150. https://doi.org/10.15554/pcij.05011987.74.150

Sharma A, Reddy GR, Eligehausen R et al (2014) Seismic response of reinforced concrete frames with haunch retrofit solution. ACI Struct J 111:1–6. https://doi.org/10.14359/51686625

Strand7 (2010) Using Strand7/Straus7. Introduction to the Strand/Straus7 Finite Element Analysis System. www.strand7.com

Tonidis M, Sharma A (2021) Numerical investigations on the influence of transverse beams and slab on the seismic behavior of substandard beam-column joints. Eng Struct 247:113123. https://doi.org/10.1016/j.engstruct.2021.113123

Uzumeri S (1977) Strength and ductility of cast-in-place beam-column joints. ACI Symp Publ 53:293–350. https://doi.org/10.14359/17701

Vecchio FJ, Collins MP (1986) The modified compression-field theory for reinforced concrete elements subjected to shear. ACI J Proc 83(2):219–231. https://doi.org/10.14359/10416

Vollum R, Newman JB (1999) Strut and tie models for analysis/design of external beam-column joints. Mag Concr Res 51(6):415–425. https://doi.org/10.1680/macr.1999.51.6.415

Wang J, Burton HV, Dai K (2019) Combination rules used to account for orthogonal seismic effects: state-of-the-art review. J Struct Eng 145(11):03119,001. https://doi.org/10.1061/(asce)st.1943-541x.0002420

Yu QS, Gross JL (2000) Seismic rehabilitation design of steel moment connection with welded haunch. J Struct 126:69–78

Yun YM, Chae HS, Kim B et al (2018) Verification of three-dimensional grid strut-and-tie model approach in structural concrete. ACI Struct J 115(1):27–40. https://doi.org/10.14359/51700946

Yun YM, Kim B, Ramirez JA (2018) Three-dimensional grid strut-and-tie model approach in structural concrete design. ACI Struct J 115(1):15–26. https://doi.org/10.14359/51700791

Publisher's Note Springer Nature remains neutral with regard to jurisdictional claims in published maps and institutional affiliations.